http://www.cns.s.u-tokyo.ac.jp/summerschool/

Exotic cluster structure in light nuclei

Naoyuki Itagaki　University of Tokyo

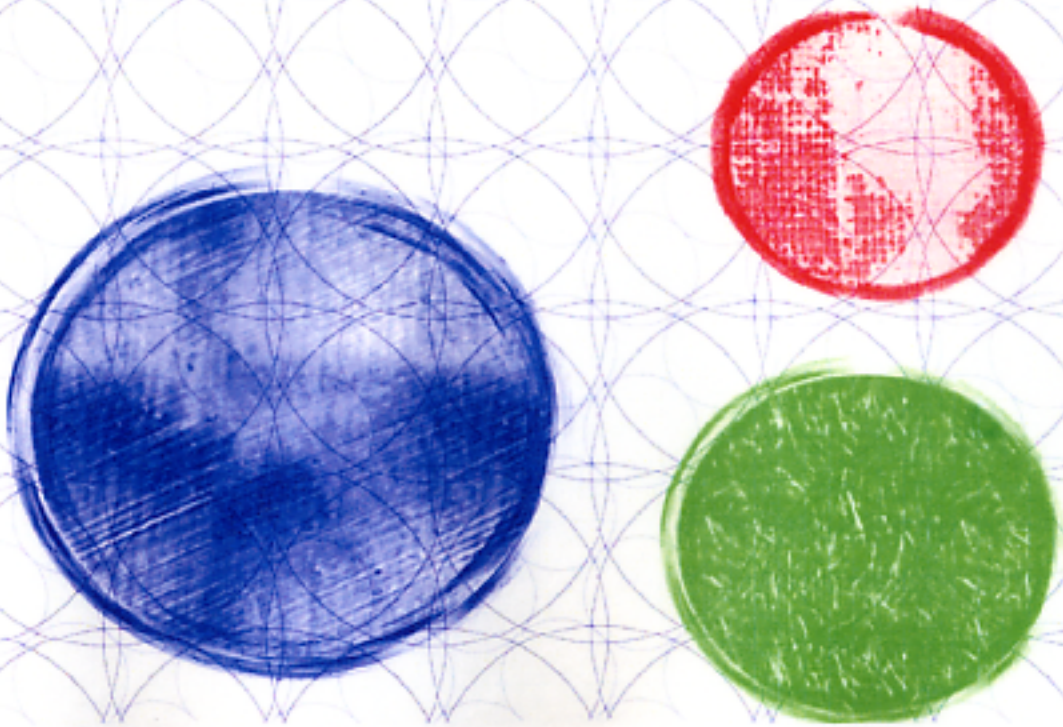

Outline of the talk

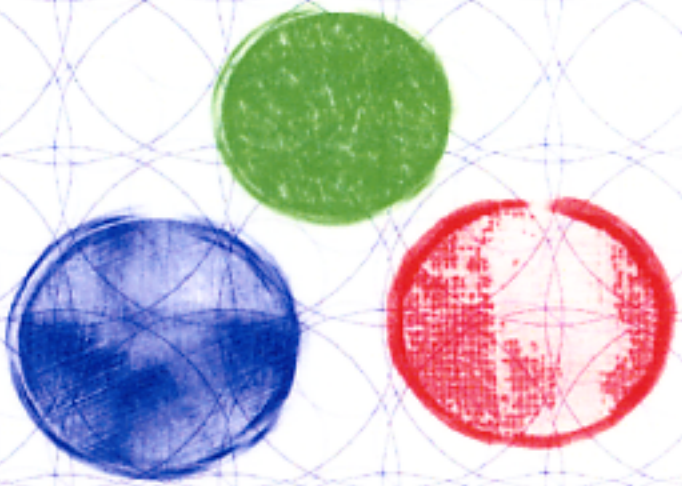

1) Basic idea

2) History of cluster theory in 4N nuclei

3) Cluster structure in neutron-rich nuclei

4) Conclusion and future perspective

Nuclei ---

Finite Quantum Many-body System
consisting of Protons and Neutrons

Structure of nuclei ---

Nucleons construct self-consistent
mean field and occupy
single-particle orbits

Mean-field Model
Shell Model

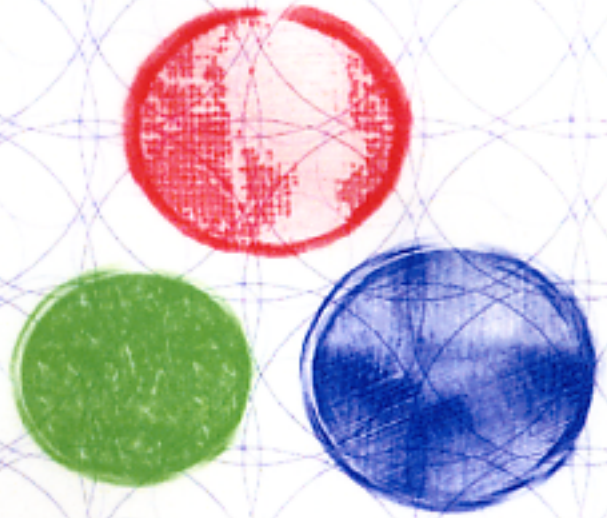

Nuclei ---

Finite Quantum Many-body System
consisting of Protons and Neutrons

Structure of nuclei ---

Nucleons construct self-consistent
mean field and occupy
single-particle orbits

Mean-field Model
Shell Model

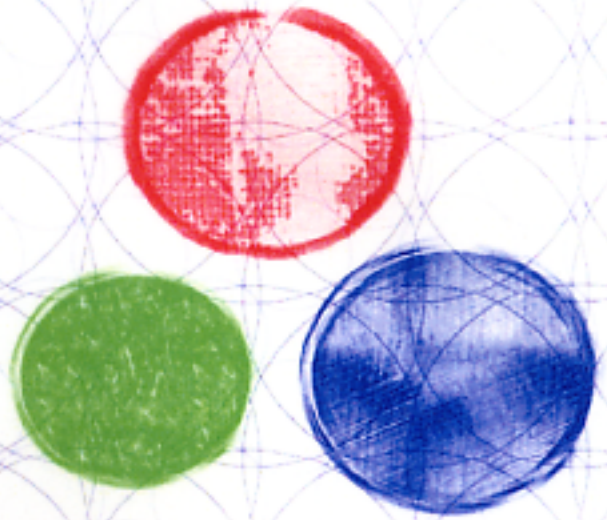

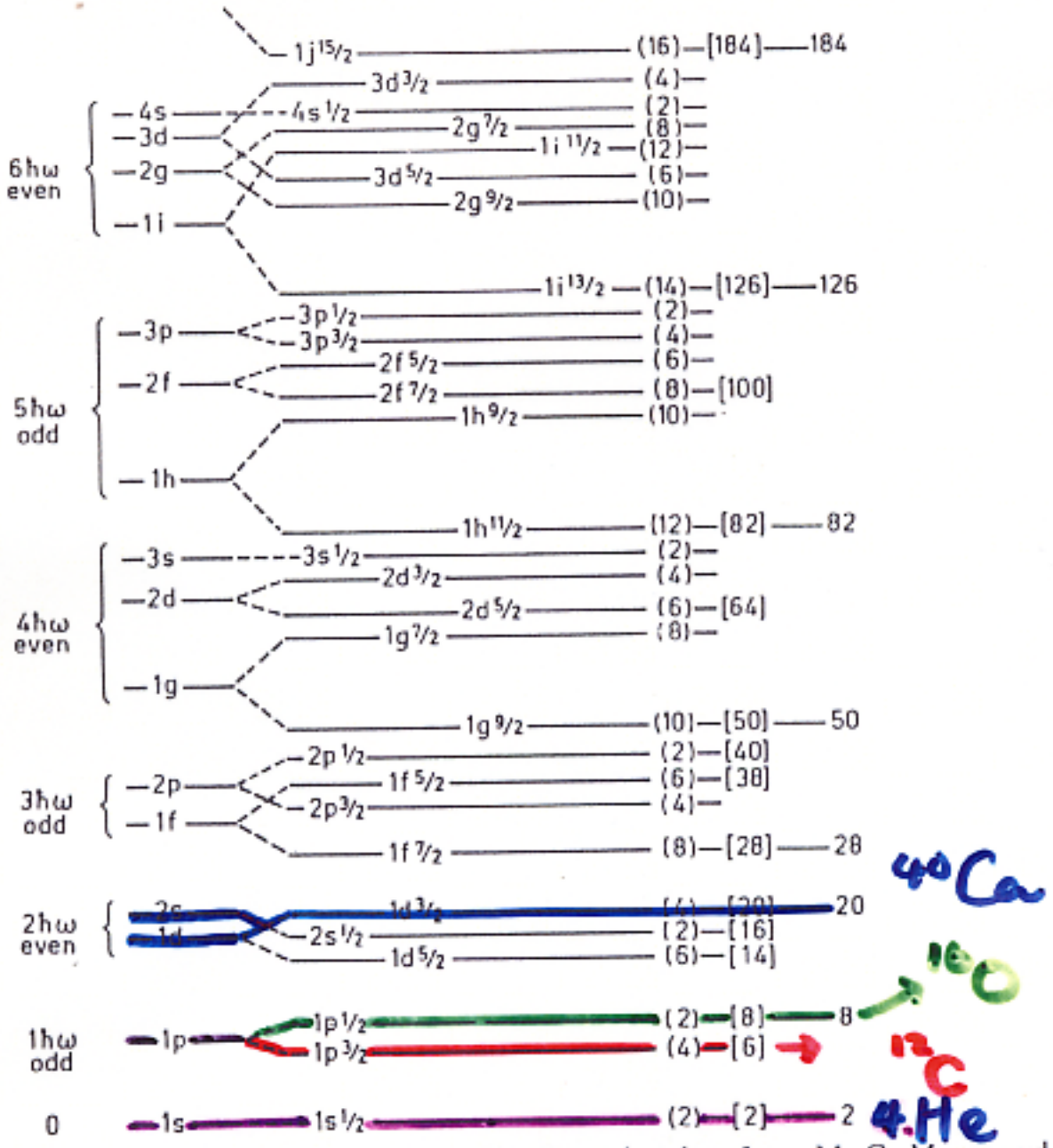

Sequence of one-particle orbits. The figure is taken from M. G. Mayer and J. H. D. Jensen, *Elementary Theory of Nuclear Shell Structure*, p. 58, Wiley, New York, 1955.

Cluster structure ---

Another phase of the nuclear structure

How it appears?

Why it appears?

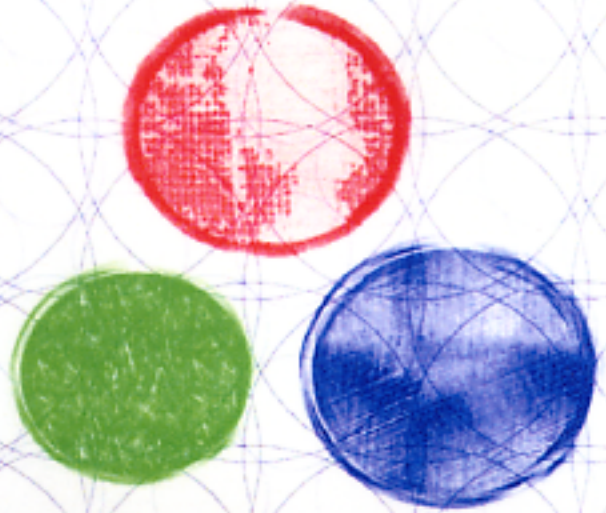

2^+; I=1 — 0 — 838 ms

$^{8}_{3}Li$

$^{8}_{4}Be$

Δ: 4941.66 *3* S_p: 18899.2 *5* S_p: 17255.0 *5* Q_α: 91.84 *4*

Populating Reactions and Decay Modes

A ^{8}Li β^- decay
B ^{8}B β^+ decay
C ^{4}He(α,γ)
D ^{4}He(α,α)
E ^{6}Li(t,n)
F ^{6}Li(^{3}He,p), (^{3}He,2α)
G ^{6}Li(α,d), (α,2α)
H ^{6}Li(^{6}Li,α), (^{6}Li,2d)
I ^{7}Li(p,γ)
J ^{7}Li(p,n)
K ^{7}Li(p,p), (p,p')
L ^{9}Be(^{3}He,α),
M ^{6}Li(d,α), (d,αp)

Levels and γ-ray branchings:

- **0**, 0^+, Γ=6.8 *17* eV, *[ABCDEFGHIL]*, %2α=100, T=0
- **3040** *30*, 2^+, Γ=1.50 *2* MeV, *[ABCDEFGHIL]*, %2α=100, T=0
- **11400** *300*, 4^+, Γ≈ 3.5 MeV, *[DGHL]*, T=0
- **16626** *3*, 2^+, Γ=108.1 *5* keV, *[BCDEFHIL]*, %2α=100, T=0+1 γ_{3040} ***1*** (t_γ100) M1
- **16922** *3*, 2^+, Γ=74.0 *4* keV, *[CDEFHIL]*, T=0+1 γ_{3040} ***13882*** (t_γ100)
- **17640** *10*, 1^+, Γ=10.7 *5* keV, *[FIK]*, T=1 γ_{16922} ***718*** (t_γ0.008 *2*) M1 γ_1 (t_γ0.019 *2*) M1+E2: δ=−0.014 *13* γ_{3040} ***14586*** (t_γ49.7 *4*) M1+E2: δ=(γ_0 ***17619*** (t_γ100) M1
- **18150** *4*, 1^+, Γ=138 *6* keV, *[FIK]*, T=0 γ_{16922} ***1228*** (t_γ1.6 *2*) M1 γ_{1662} (t_γ2.0 *5*) M1 γ_{3040} ***15095*** (t_γ100) M1 γ_0 ***18128*** (t_γ79) M1
- **18910**, 2^-, Γ=122 keV, *[FIJK]* γ_{16922} ***1988*** (t_γ59) E1 γ_{16626} ***2284*** (t
- **19070** *30*, 3^+, Γ=270 *20* keV, *[FIK]*, T=(1) γ_{3040} ***16013*** (t_γ100) M1
- **19240** *25*, 3^+, Γ=230 *30* keV, *[JKL]*, T=(0)
- **19400**, 1^-, Γ≈ 650 keV, *[FJK]*
- **19860** *50*, 4^+, Γ=0.7 *1* MeV, *[DFL]*, T=0
- **20100**, 2^+, Γ≈ 1.1 MeV, *[DJK]*, T=0
- **20200**, 0^+, Γ<1 MeV, *[D]*, T=0
- **20900**, 4^-, Γ=1.6 *2* MeV, *[K]*
- **21500**, $3(^+)$, Γ=1 MeV, *[IJ]*
- **22000**, 1^-, Γ≈ 4 MeV, *[I]*, T=1
- **22050** *100*, Γ=270 *70* keV, *[L]*

J = 0, 2, 4

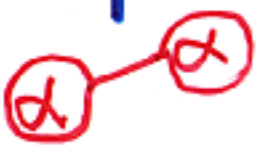

$E_x = \frac{\hbar^2}{2I} J(J+1)$

40000
36000
32000

Mechanisms of (α)-clustering

^{4}He -- strongly boud system

B.E./A=7.1MeV

^{4}He-^{4}He -- weakly interacting

Unit of structures

^{8}Be	$\alpha + \alpha$	-0.1MeV	
^{12}C	$\alpha + \alpha + \alpha$	+7.2MeV	
^{20}Ne	^{16}O+ α	+4.7MeV	

Threshold Rule

Cluster structure ---

Why it appears?

It is another way for nuclei
to be excited with low cost (energy)

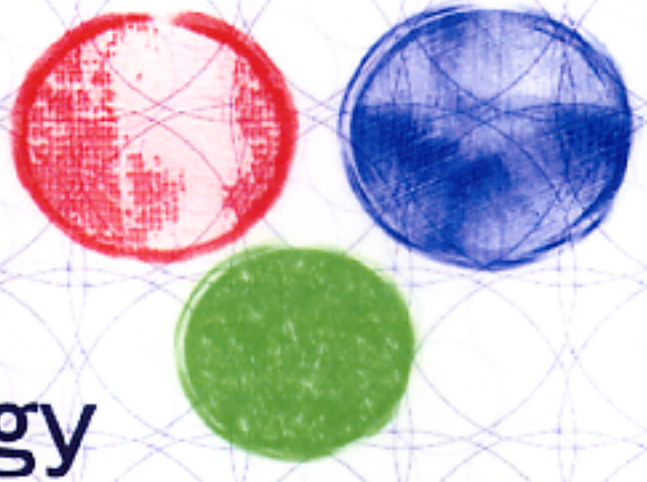

sometimes
the excitation energy
is lower than the ph excitation case

Mysterious 0^+ state in ^{16}O

The ground 0^+ state --- closed p-shell

The first excited state -- 0^+ at 6.049 MeV

2p-2h excitation to the sd-shell?

c.f. ^{15}O

$1/2^-$ state is the ground state

$1/2^+$ state is at 5.183 MeV

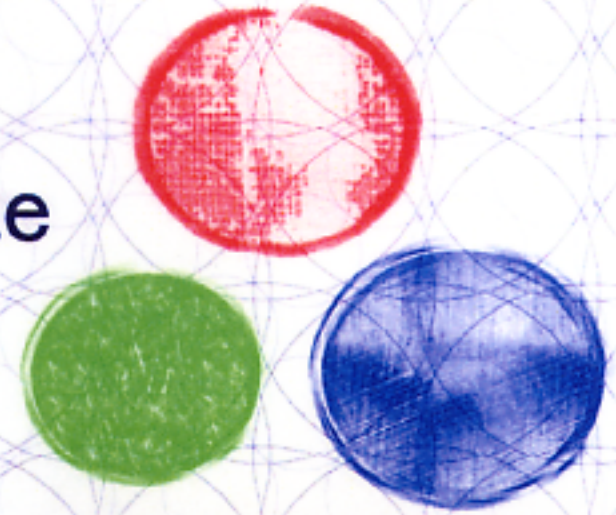

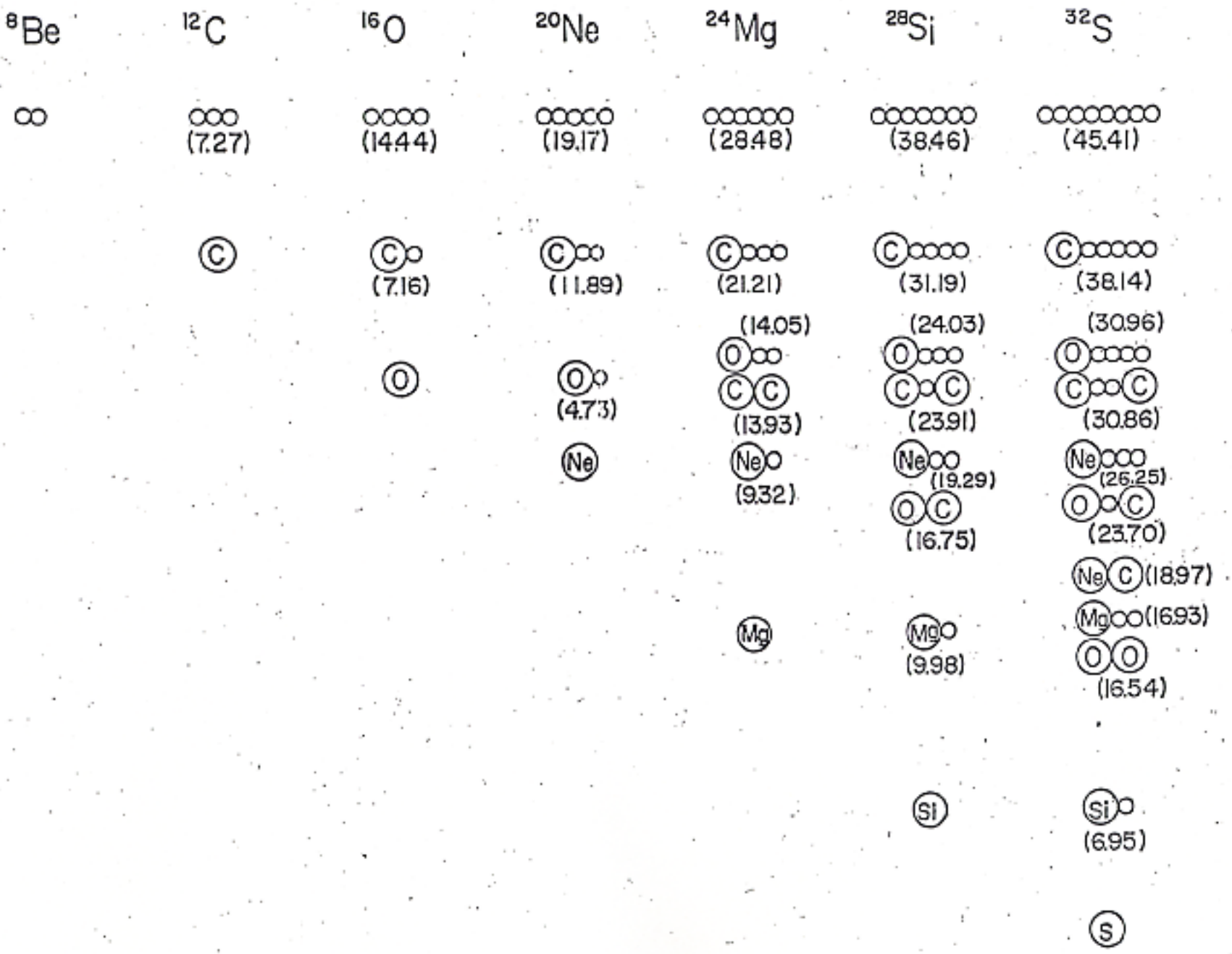

Fig. 1. The Ikeda diagram which shows the subunits of the possible molecule-like structures expected to appear near the respective threshold energies for the break-up into subunit nuclei. The threshold energies are written in parentheses.

Inversion doublet (parity doublet) structure (by Horiuchi, Ikeda)

Cluster – Cluster interaction is weak

↓

Cluster – Cluster potential is shallow

↓

relative wave function can increase the number of node with low energy

rotational bands of positive-parity and negative-parity almost degenerate

ıı energy of 15 MeV.

eight negative-parity $T=0$ states below the
nd many $T=0$ states above this as shown in

arity
/)

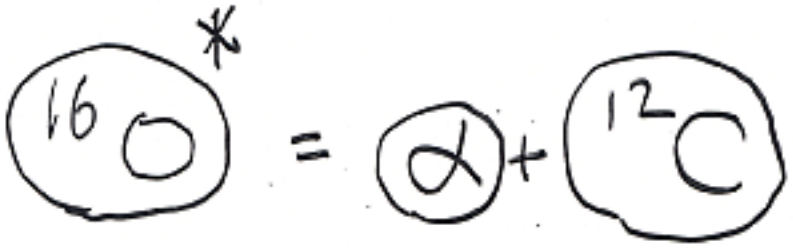

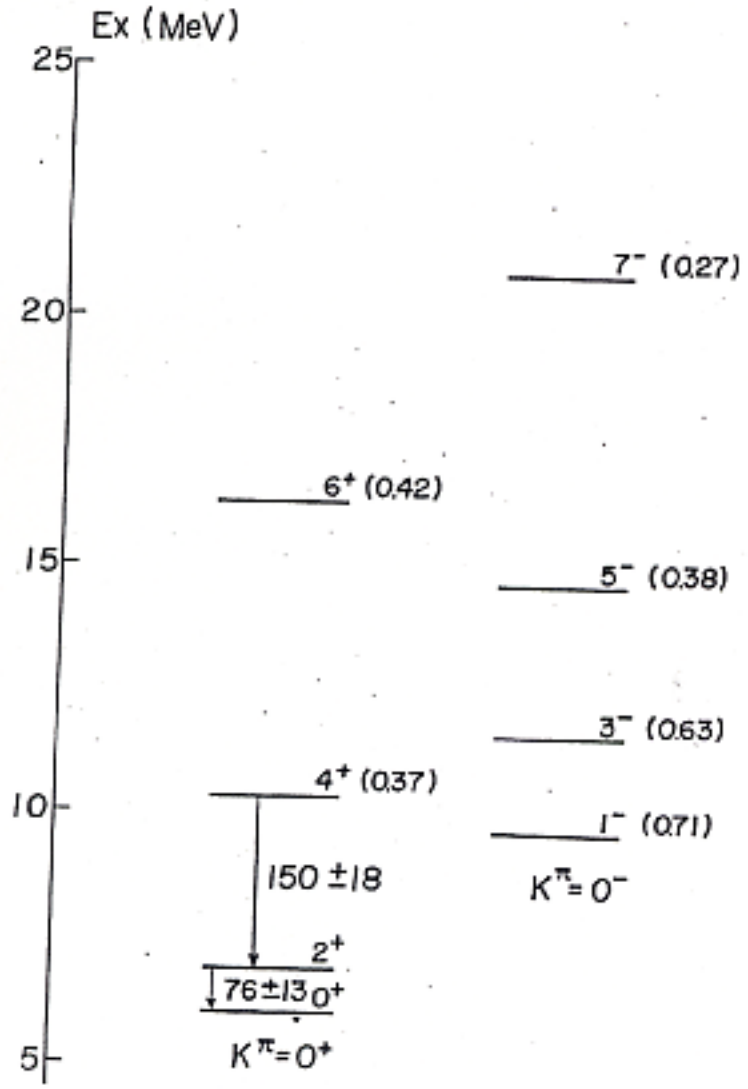

Fig. 1-3. The rotational bands in ^{16}O. The values in parentheses are the dimensionless reduced α-widths at a channel radius 5.2 fm. The $B(E2)$ values are in unit of $e^2\,\mathrm{fm}^4$.

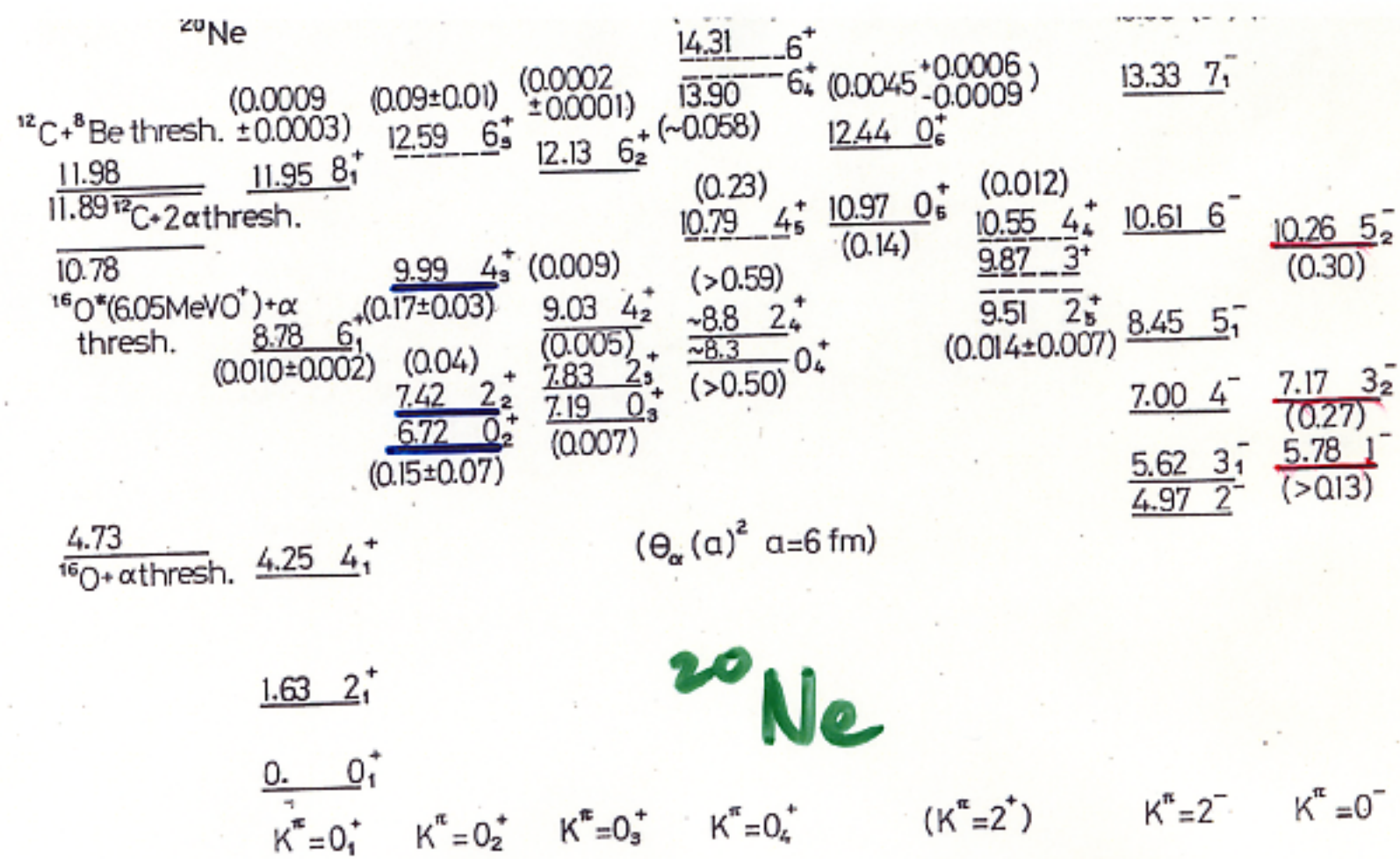

Fig. 1-5. Low-lying $T=0$ energy levels of ^{20}Ne with excitation energies in MeV and with reduced α-widths ($\theta_\alpha(a)^2$) at the channel radius $a=6$ fm. The excitation energies and the α-decay widths are taken from Ref. 91) except those of the 12.44 MeV 0_6^+ state (Ref. 92)). Almost all the levels below about 10 MeV excitation are classified into rotational bands. The dashed bars denote tentative band assignment. The $(sd)^4$ shell model reproduces the $K^\pi=0_1^+$ and 0_2^+ bands, the ^{16}O+α cluster model the $K^\pi=0_1^+$, 0_4^+ and 0^- bands, the ESM (MRGM) and the α-^{12}C-α GCM the $K^\pi=0_1^+$, 0_2^+, 0_4^+ and 0^- bands, and the (^{16}O-α) + (^{12}C-^{8}Be) CCOCM and the ^{12}C+2α OCM the $K^\pi=0_1^+$, 0_2^+, 0_3^+, 0_4^+, 2^- and 0^- bands.

(0_2^+ (6.72 MeV), 0_3^+ (7.19 MeV), 0_4^+ (~8.3 MeV), 2^- (4.97 MeV)

The formation of ^{12}C

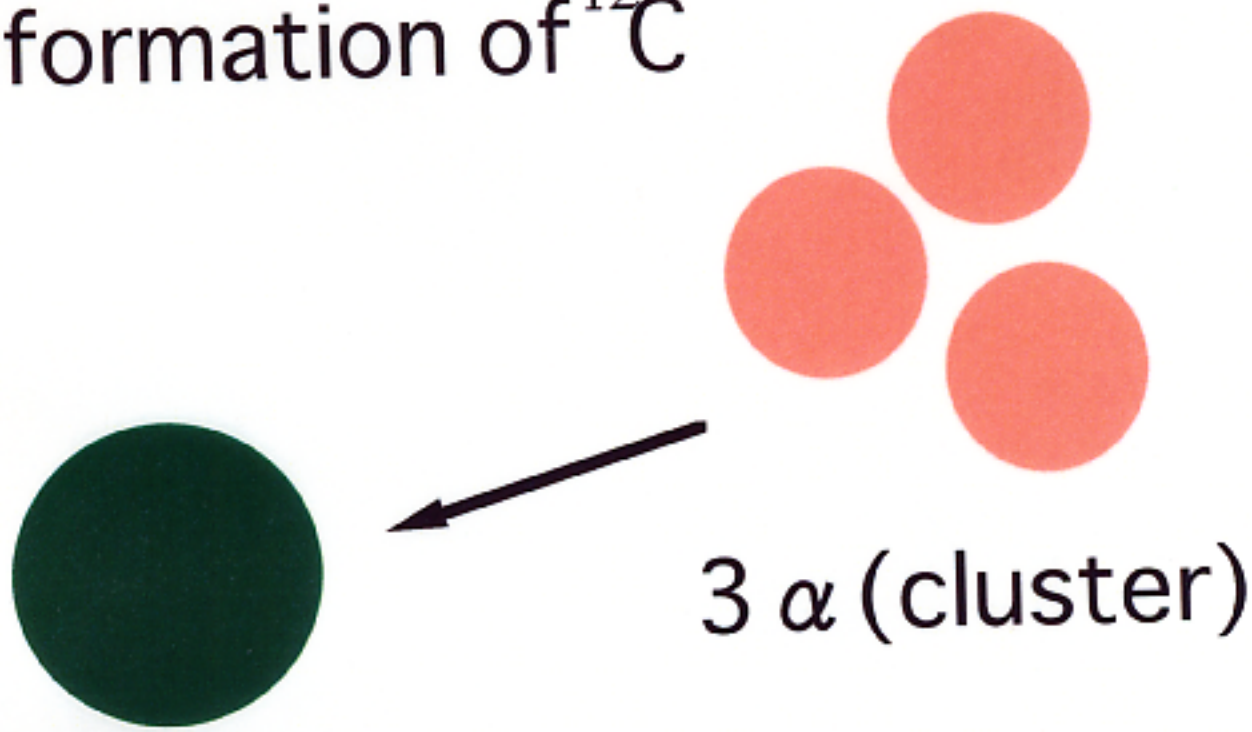

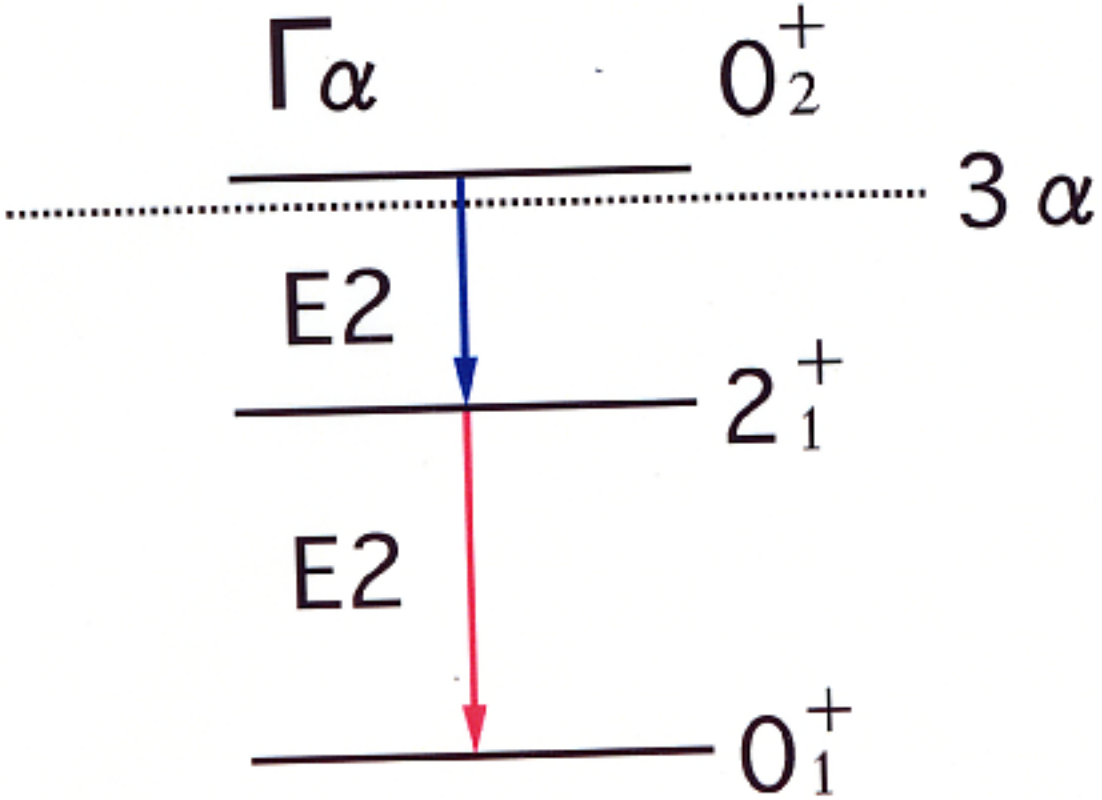

CM calculations and 0.2515 fm^{-2} ($b=1.41$ fm) in the GCM cal
the experimental value[165] is known to be 0.285 fm^{-2}. The si
's in ^{12}C is inspected by the variational calculation versus ν_0 i
ese choices are found to be good.

Energy spectra and structure of ^{12}C

Sapple of P.T.P. No. 68 (1980

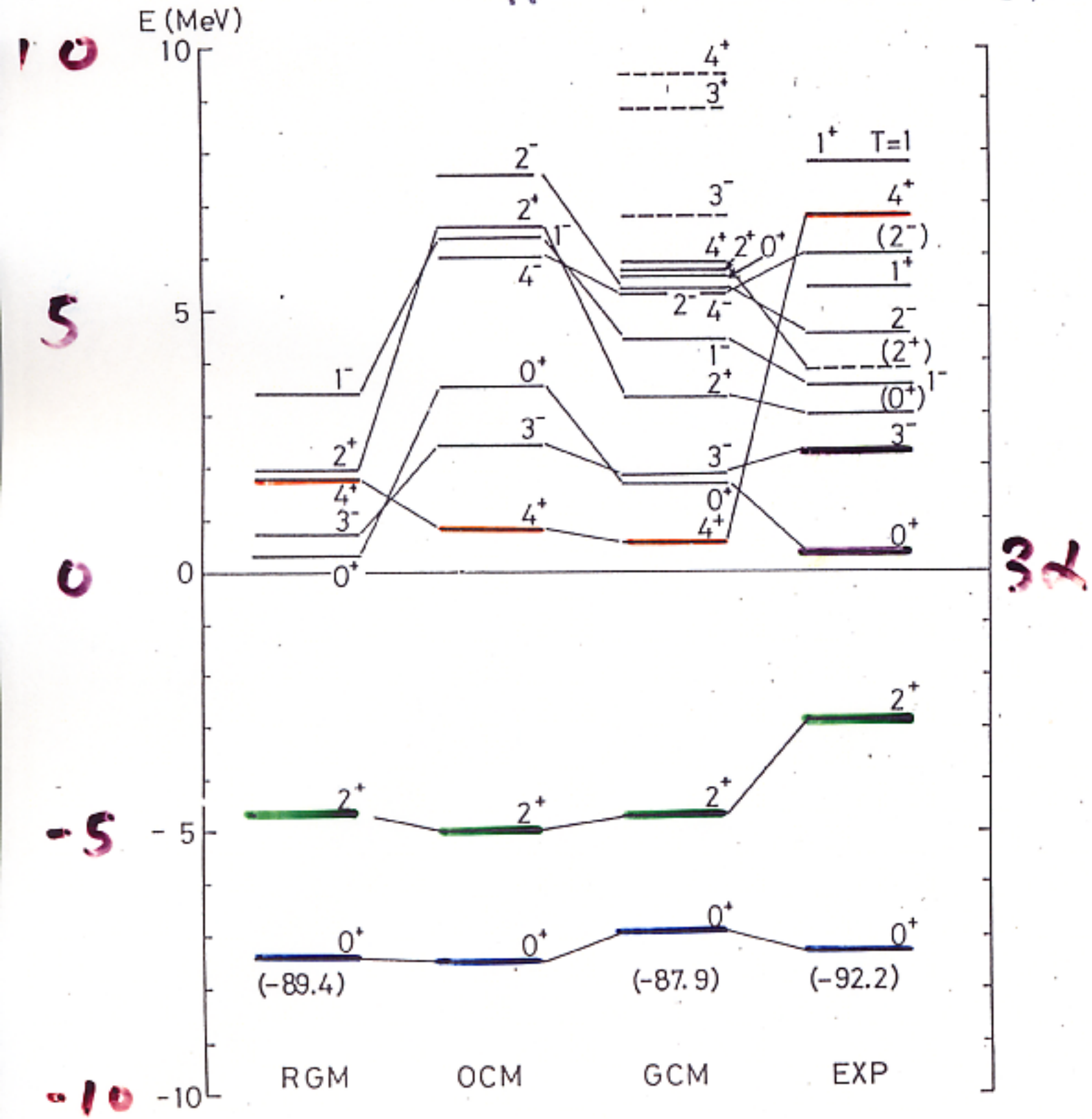

2-2. Calculated energy spectra of ^{12}C and the experimental one.[16] The r

E. Uegaki Y. Abe S. Okabe and H. Tanaka
P.T.P 59 (1978) 1031

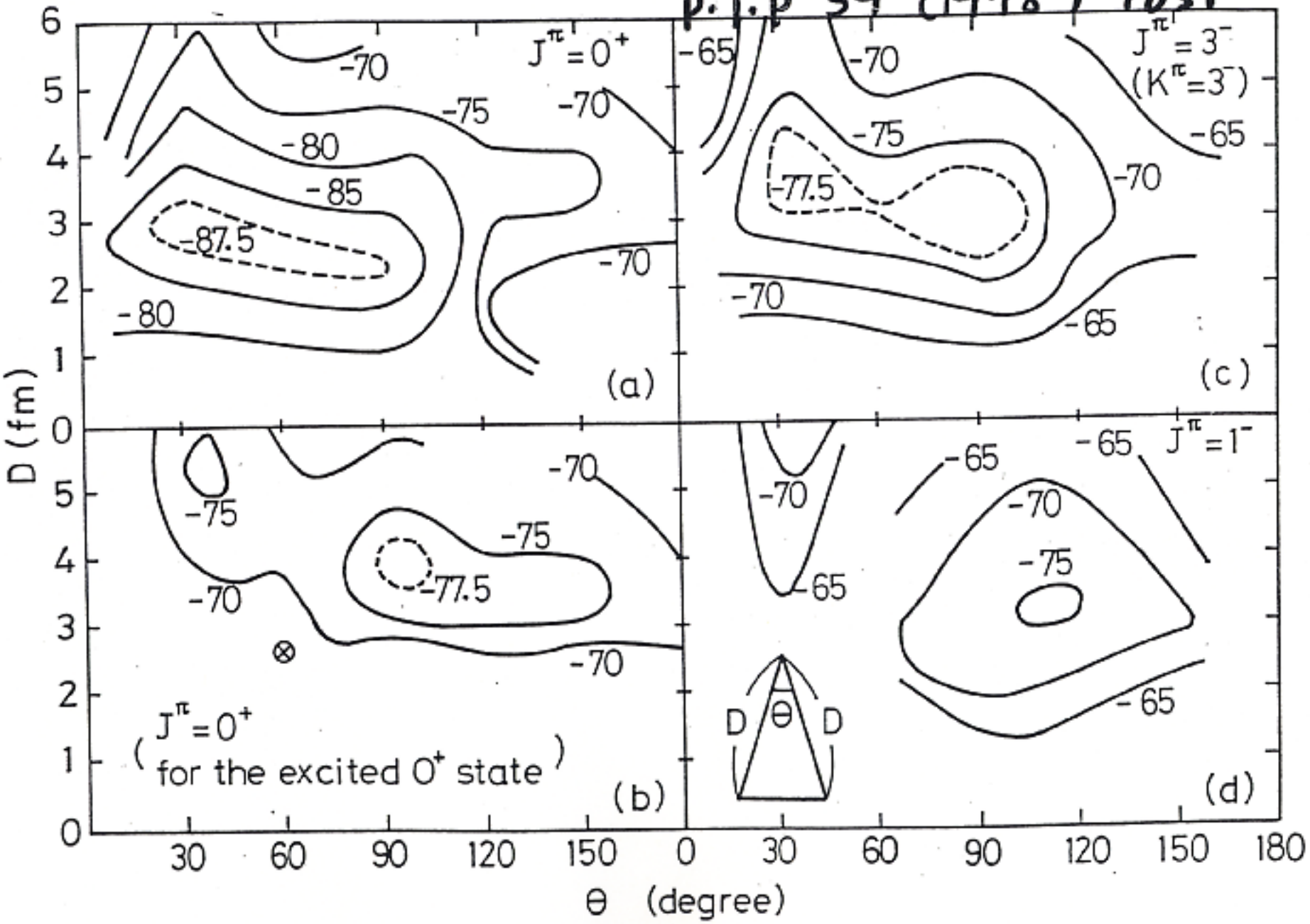

Fig. 2-3. Energy surfaces in the isosceles configuration (for D and θ, see the illustration in (d)). The Volkov No. 1 (m=0.60) force is used without the Coulomb force. (a)

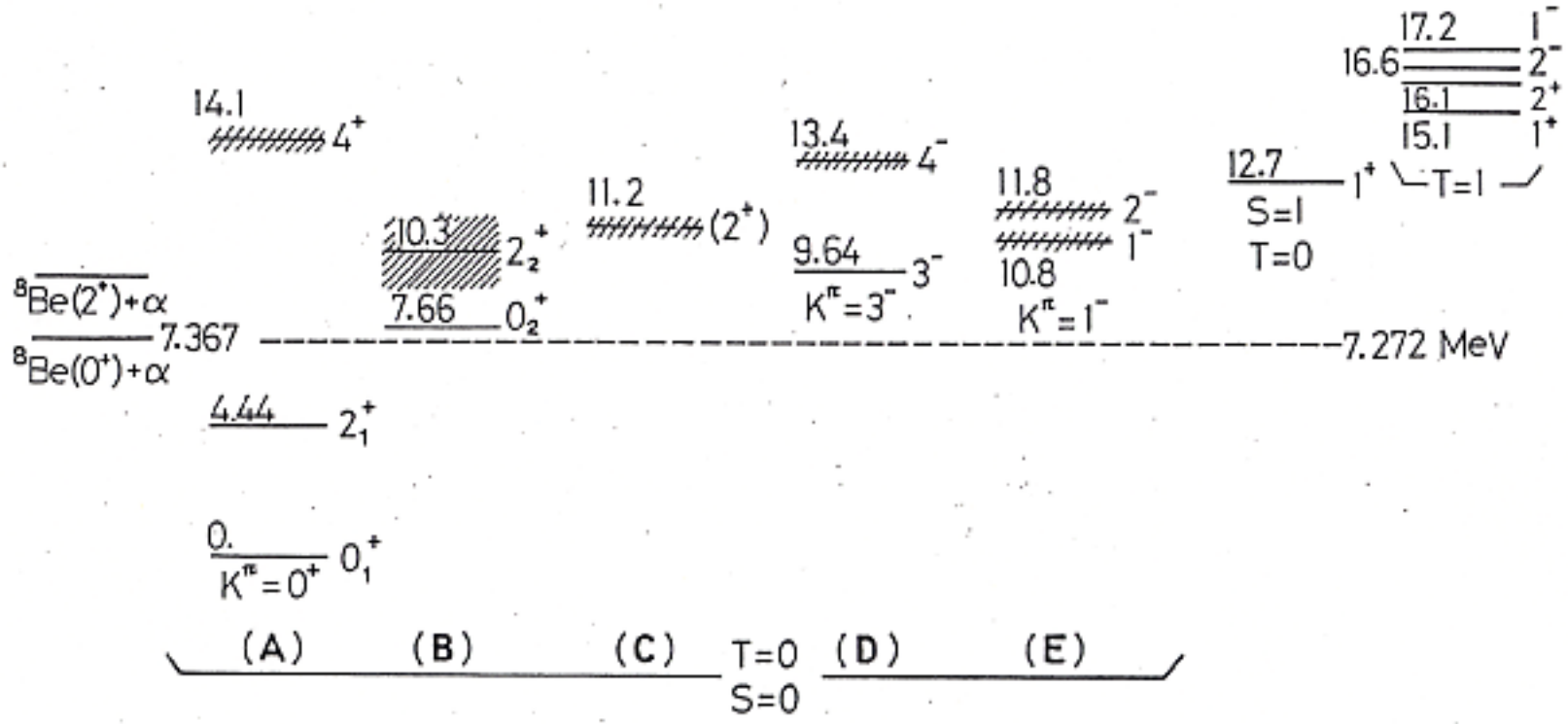

Fig. 1-1. Experimental energy levels of ^{12}C are classified into several bands according to the dynamical calculations in § 2. (A) $K^\pi=0^+$ ground rotational band, (B) the first family of the excited positive-parity states including the 0_2^+ and 2_2^+ states, (C) the second family of excited positive-parity states. (D) shows $K^\pi=3^-$ band, (E) $K^\pi=1^-$ band. The data are taken from Ref. 16). Here, the (0^+) level at 10.3 MeV and the (2^-) level at 13.35 MeV are assigned to $J^\pi=2^+$ and 4^- respectively, according to the dynamical calculations in § 2.

same problem by the hybrid model where the broken symmetry ([4²31]) configuration of $0p$-shell shell model were introduced besides the 3α-clustering

and an α-decay width from the 0_2 state. The present model [illegible] transition probability of $11.5e^2fm^4$ to the experimental value of $13\pm4e^2fm^4$ and the α-decay width of 7.3eV to the experimental value of 8.5 ± 1.0eV.

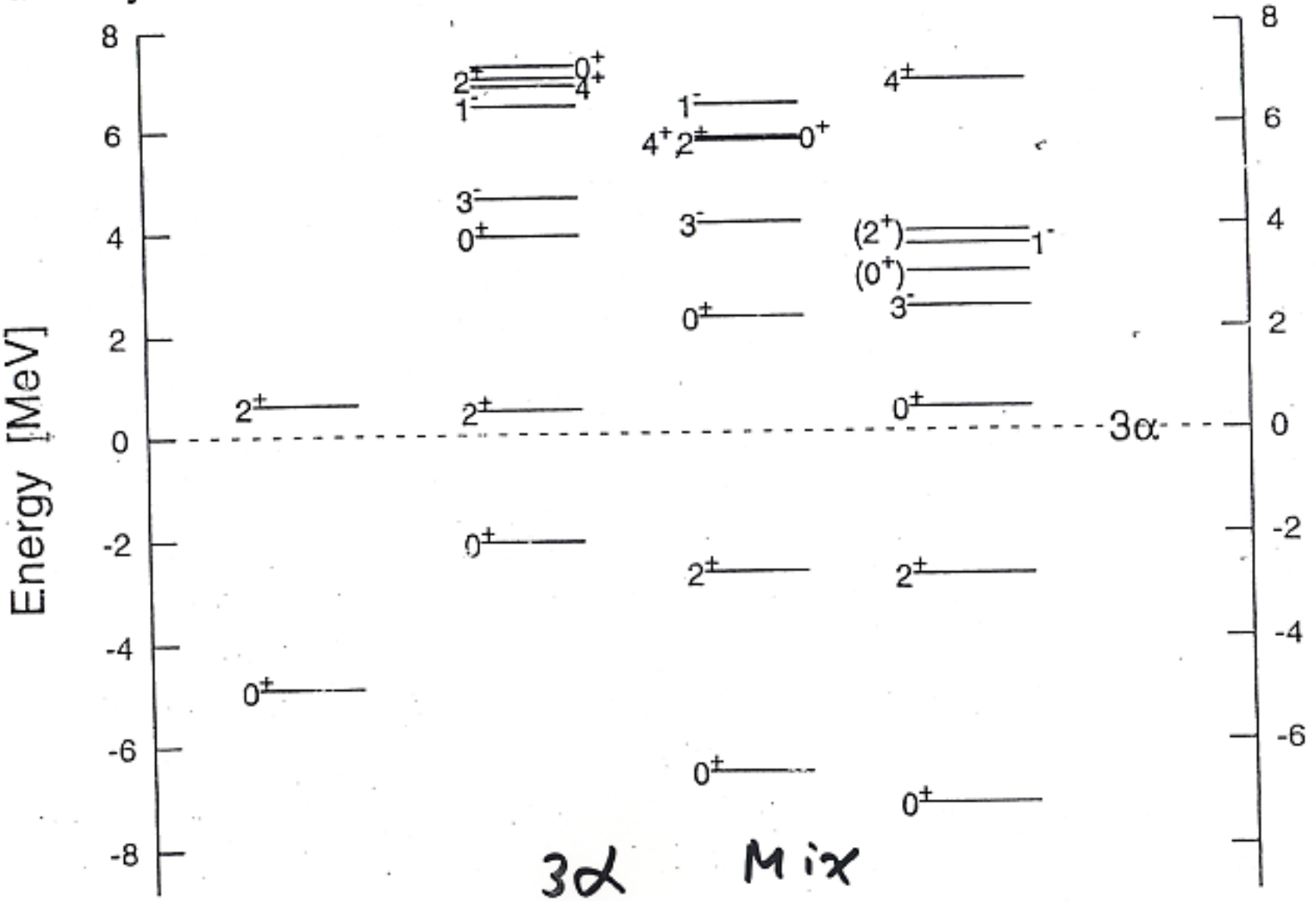

Fig.3 Energy spectrum of ^{12}C

History of the cluster calculation

phenomenological α-particle model

binding energy of 4N nuclei are
just the number of bonds of $\alpha-\alpha$?

Brink model (～1960)

microscopic calculation for light 4N nuclei
～1970-1980

microscopic calculation for nuclei
consisting of cluster(s) and valence particles
～1980

AMD (～1990)
Green Function Monte Carlo

Brink Model

$$\Psi = P\,[\,A(\phi 1\ \phi 2\ \cdots)\,]$$

$$\phi i(r) = \exp[-\nu(\vec{r} - \vec{R}i)^2]\ \chi i$$

P: Angular momentum and parity projection

A: Antisymmetrizer

$$\exp[-\nu(\vec{x} - \vec{X})^2] = (\Sigma(\sqrt{\nu}X)^n Hn(x) / n!)e^{-\nu x^2}$$

Local Gauss is equal to the coherent state of many ph states in the shell model picture

Two nucleons case (with the same spin–isospin)

$$\phi 1(r) = \exp[-\nu(\vec{r} - \vec{X})^2] \quad \chi i$$

$$\phi 2(r) = \exp[-\nu(\vec{r} + \vec{X})^2] \quad \chi i$$

$$\psi 1(r) = \phi 1(r) + \phi 2(r)$$

$$\psi 2(r) = [\phi 1(r) - \phi 2(r)] \; / \; X$$

$$A(\phi 1(r) \; \phi 2(r)) = A(\psi 1(r) \; \psi 2(r))$$

$X \longrightarrow 0$

$$\phi 1(r) = \exp[-\nu r^2] \quad \chi i$$

$$\phi 2(r) = x \exp[-\nu r^2] \quad \chi i$$

Cluster model space coincides with the lowest shell model at $X \longrightarrow 0$

~ 1985 revolution of RNB experiment

Cluster structure survives in n-rich isotopes?

Findings of the halo structure and
disappearance of the magic number
are related to the s-wave problem

The possibility that the cluster structure
becomes more important due to
the valence neutrons around it

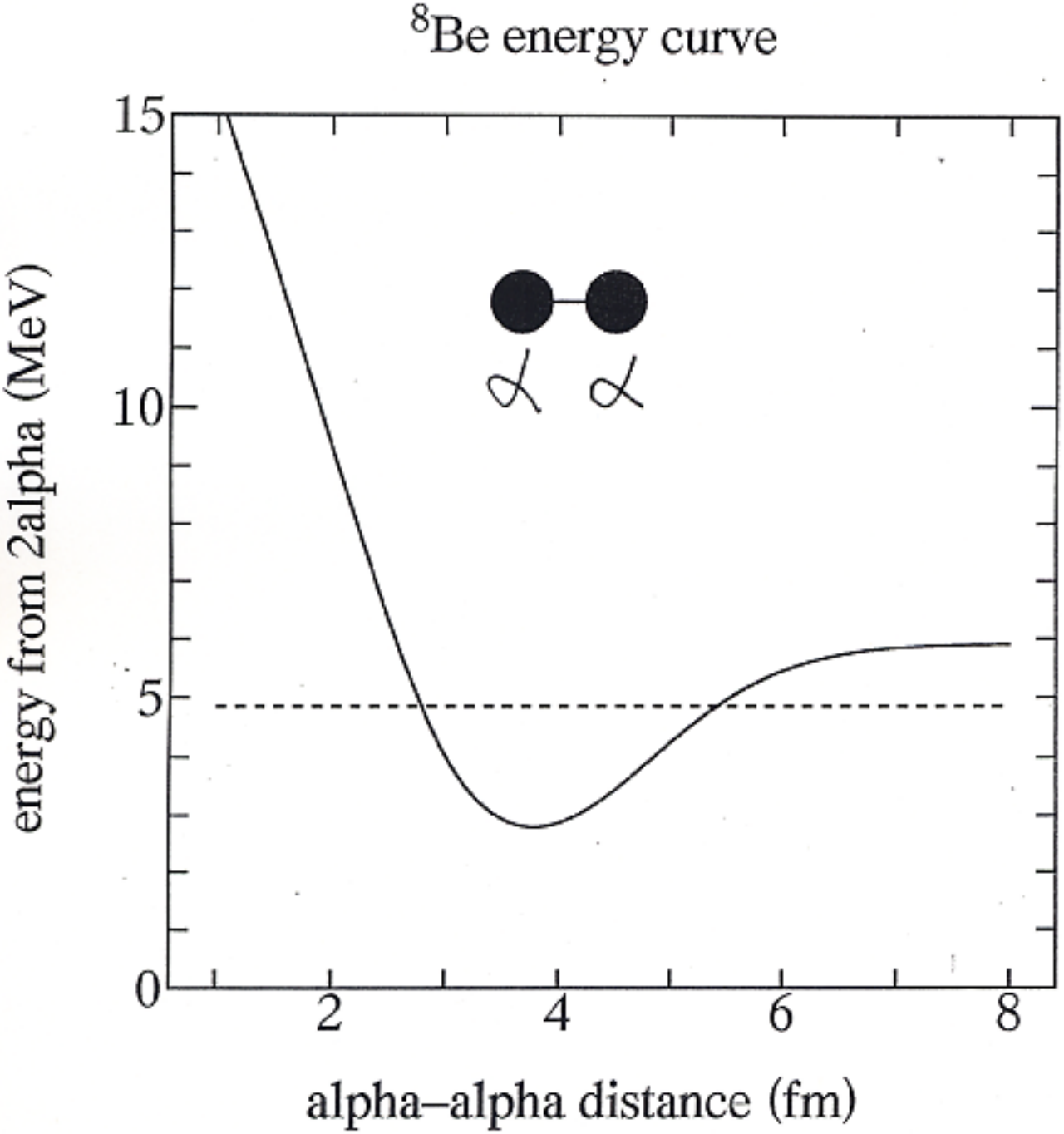
^{8}Be energy curve
15
10
5
0
2
4
6
8
energy from 2alpha (MeV)
alpha–alpha distance (fm)
α
α

A. Bohr and B.R. Mottelson
Nuclear Structure Vol. II

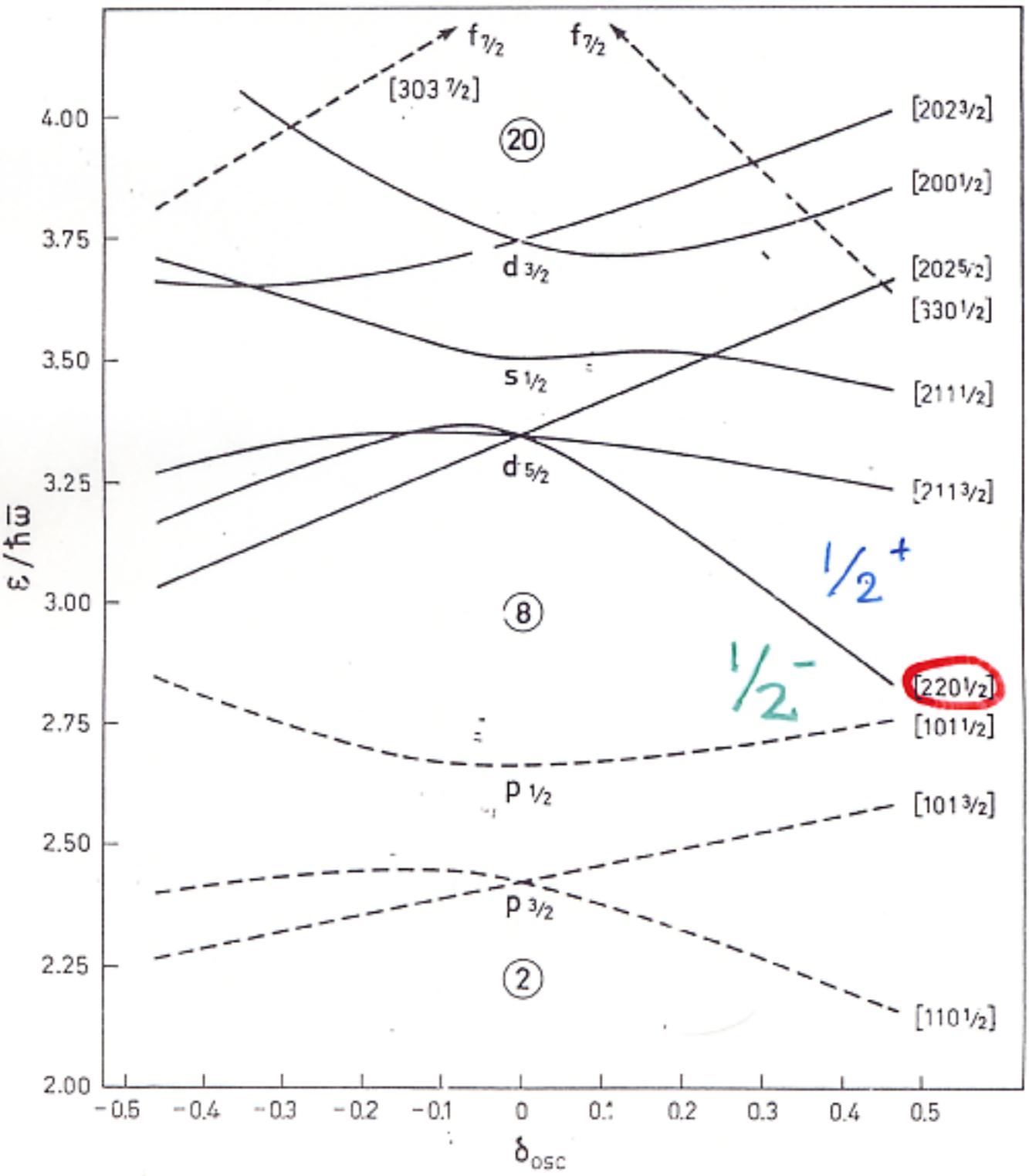

Figure 5-1 Spectrum of single-particle orbits in spheroidal potential (N and $Z < 20$). The spectrum is taken from B. R. Mottelson and S. G. Nilsson, *Mat. Fys. Skr. Dan. Vid. Selsk.* **1**, no. 8 (1959). The orbits are labeled by the asymptotic quantum numbers $[Nn_3\Lambda\Omega]$ referring to large prolate deformations. Levels with even and odd parity are drawn with solid and dashed lines, respectively.

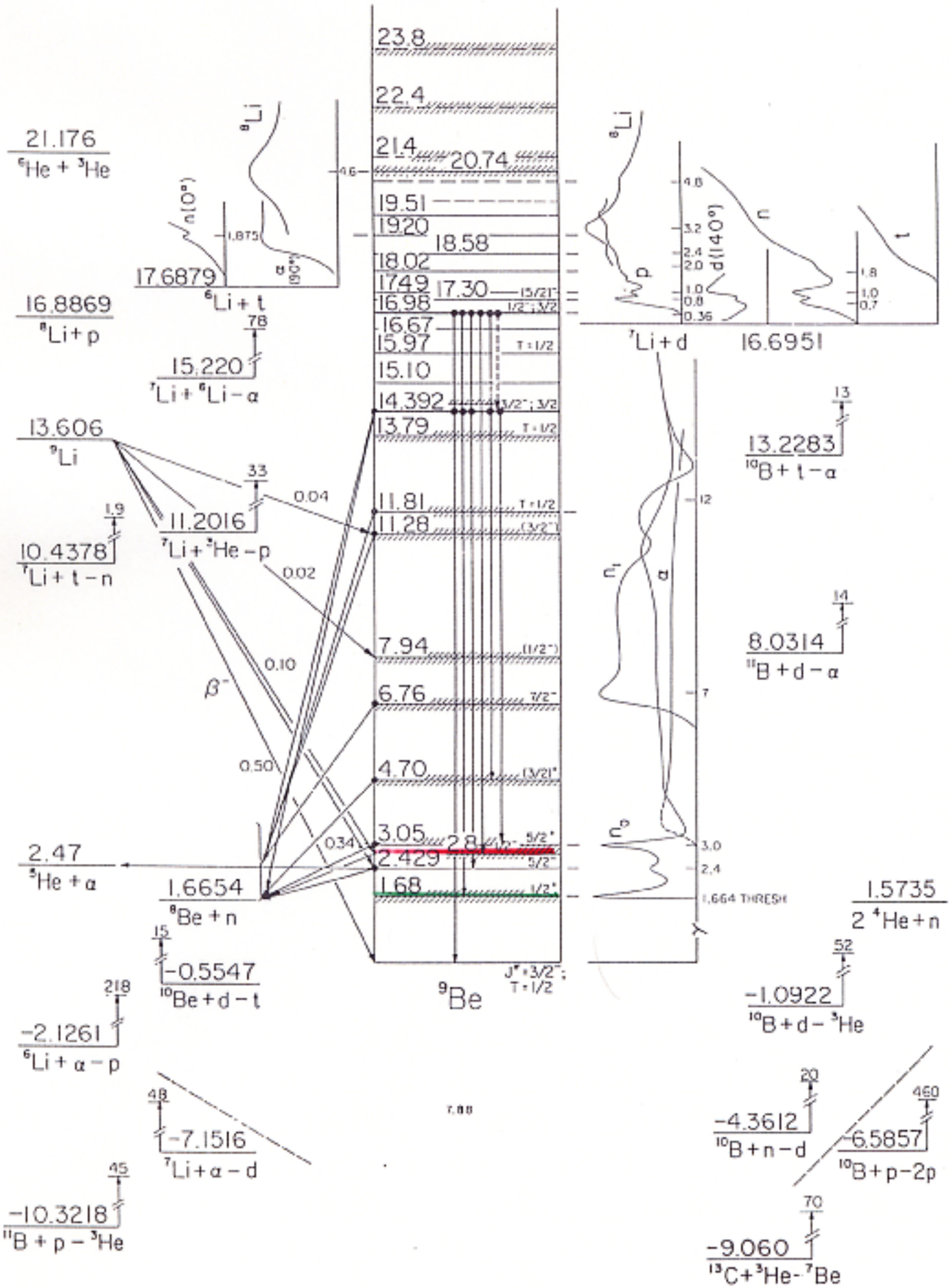

Fig. 16. Energy levels of ^{9}Be: for notation, see fig. 1.

$^9Be = \alpha + \alpha + n$

Fig. 3-2. Motion of valence neutron. The upper figures are for $1/2^+$ state and the lowers for $3/2^-$ state. (a) and (b): Contour maps of the total binding energy in MeV. Cross mark (×) denotes a position of an α-particle. (c) and (d): *Two-dimensional reduced width amplitudes* $|Z^{J^\pi}_{Lt_j}(a)|_{a_y=0}$ for $1/2^+$ $(K=1/2, \mu=1/2)$ and $3/2^-$ $(K=3/2, \mu=1/2)$ cofigurations. Dotted line in (c) denotes nodal points. (e) and (f): The total energy curves vs R in the weak-coupling scheme $[L(^8\mathrm{Be})\otimes l_j(n)]$. (g) and (h): Neutron reduced width amplitude $\gamma^{J^\pi}_{Lt_j}(a)$. (Solid line: $2\alpha+n$ method. Broken line: LCAO approximation.)

S. Okabe and Y. Abe
P.T.P. 61, 1049 (1979)

(a) π-orbit One node

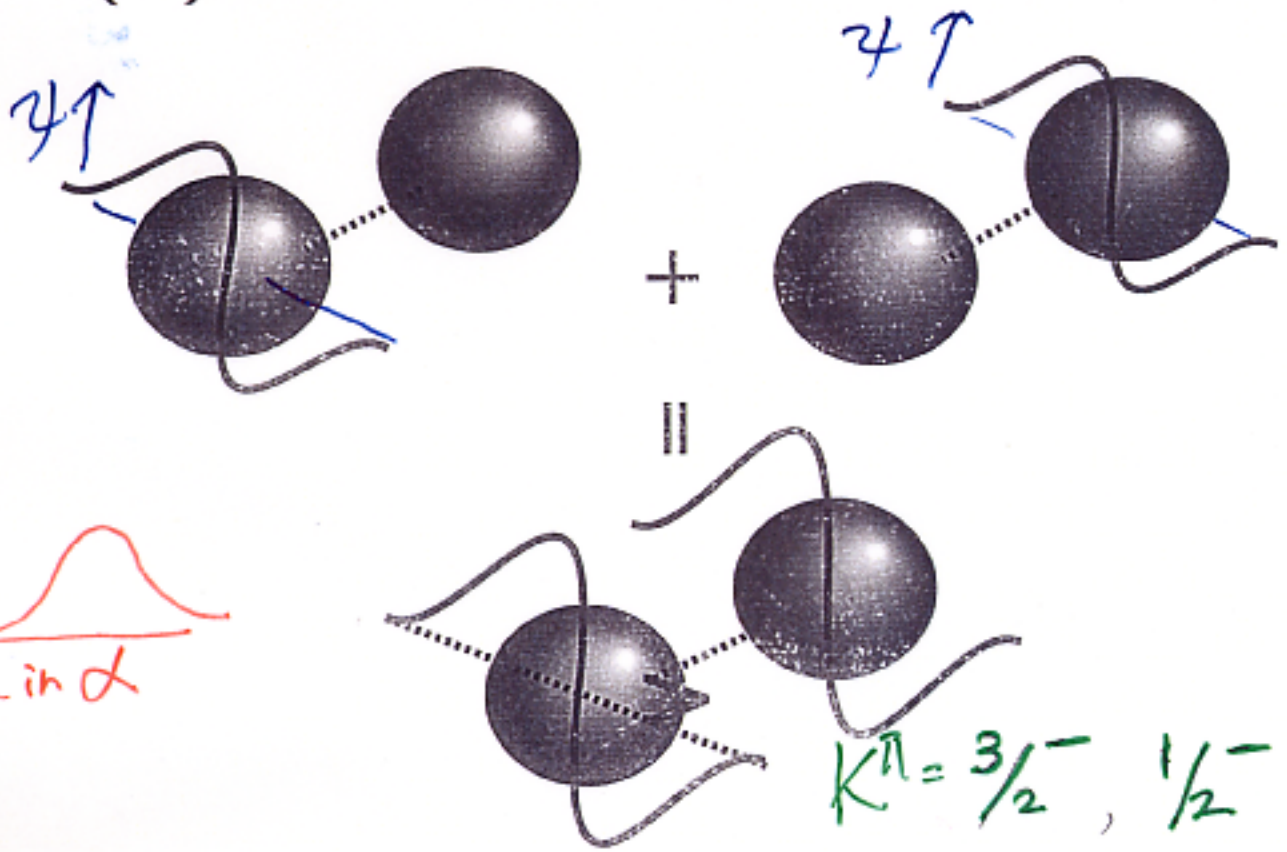

(b) σ-orbit Two nodes

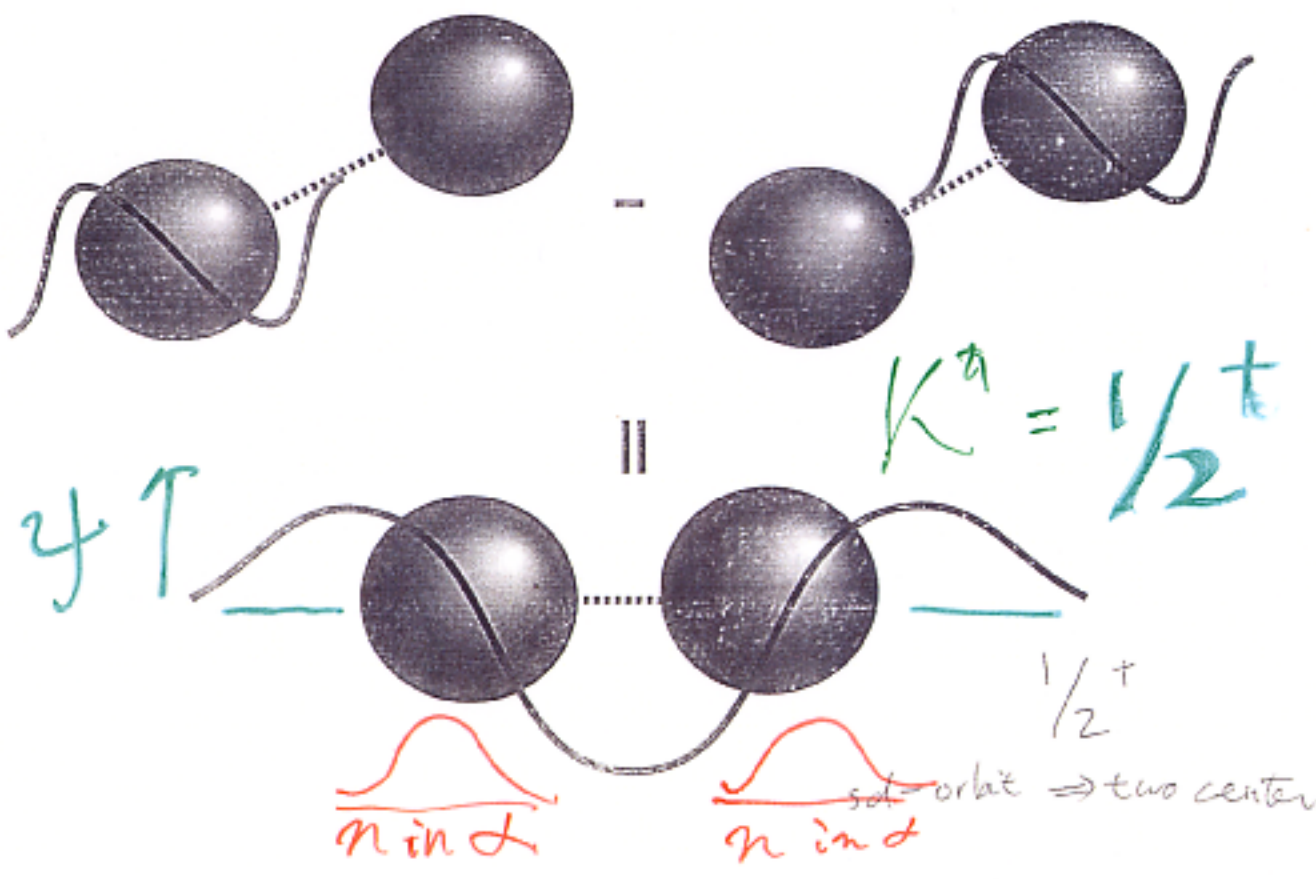

Y. Kanada-En'yo H. Horiuchi and A. Ono
Phys. Rev. C52 628 (1995)

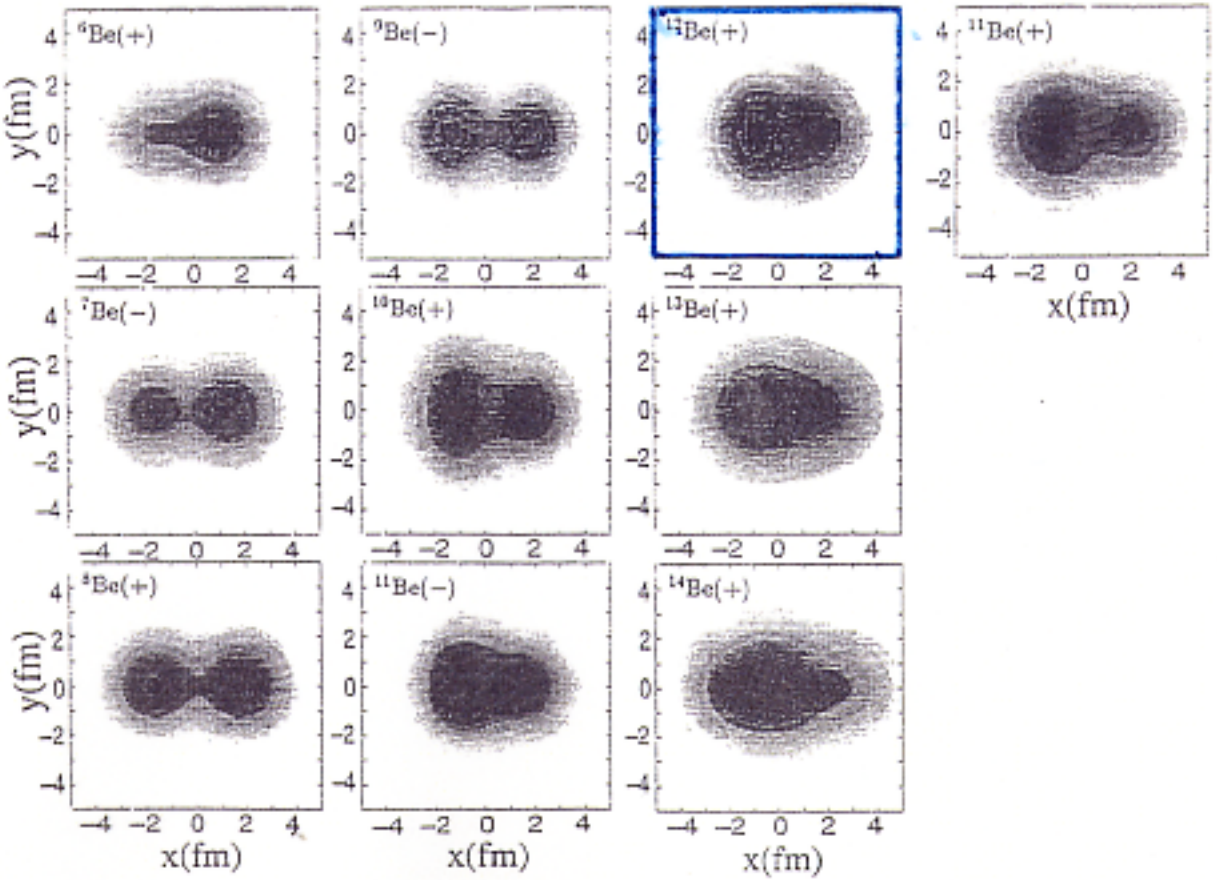

FIG. 9. Matter density distribution of AMD states of Be isotopes. The intrinsic density before parity projection is shown. Density is projected to a x-y plane and integrated along the z axis perpendicular to the plane. Units of x and y axes are in fm.

Europhys. Lett., 34 (1) (1996) 7,

^{7}Li(^{7}Li, α ^{6}He)α
^{7}Li(^{7}Li, $\alpha\alpha$)^{6}He

^{7}Li (^{7}Li, α ^{9}Be) n

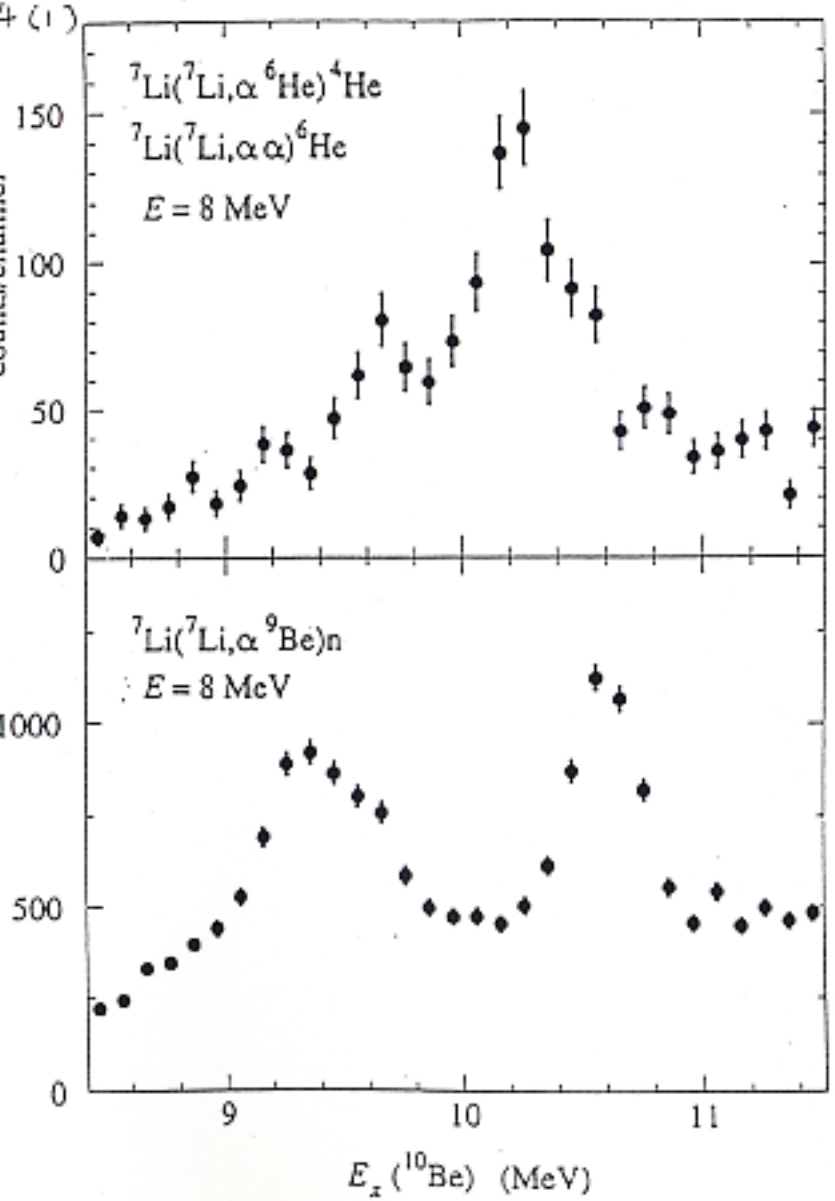

Fig. 3. – ^{10}Be excitation spectra obtained from the ^{7}Li(^{7}Li, α^6He)^{4}He and ^{7}Li(^{7}Li, α^9Be)n reactions at E_i = 8 MeV (the large difference in the number of events for these two processes is mainly due to the larger ^{9}Be detector solid angle).

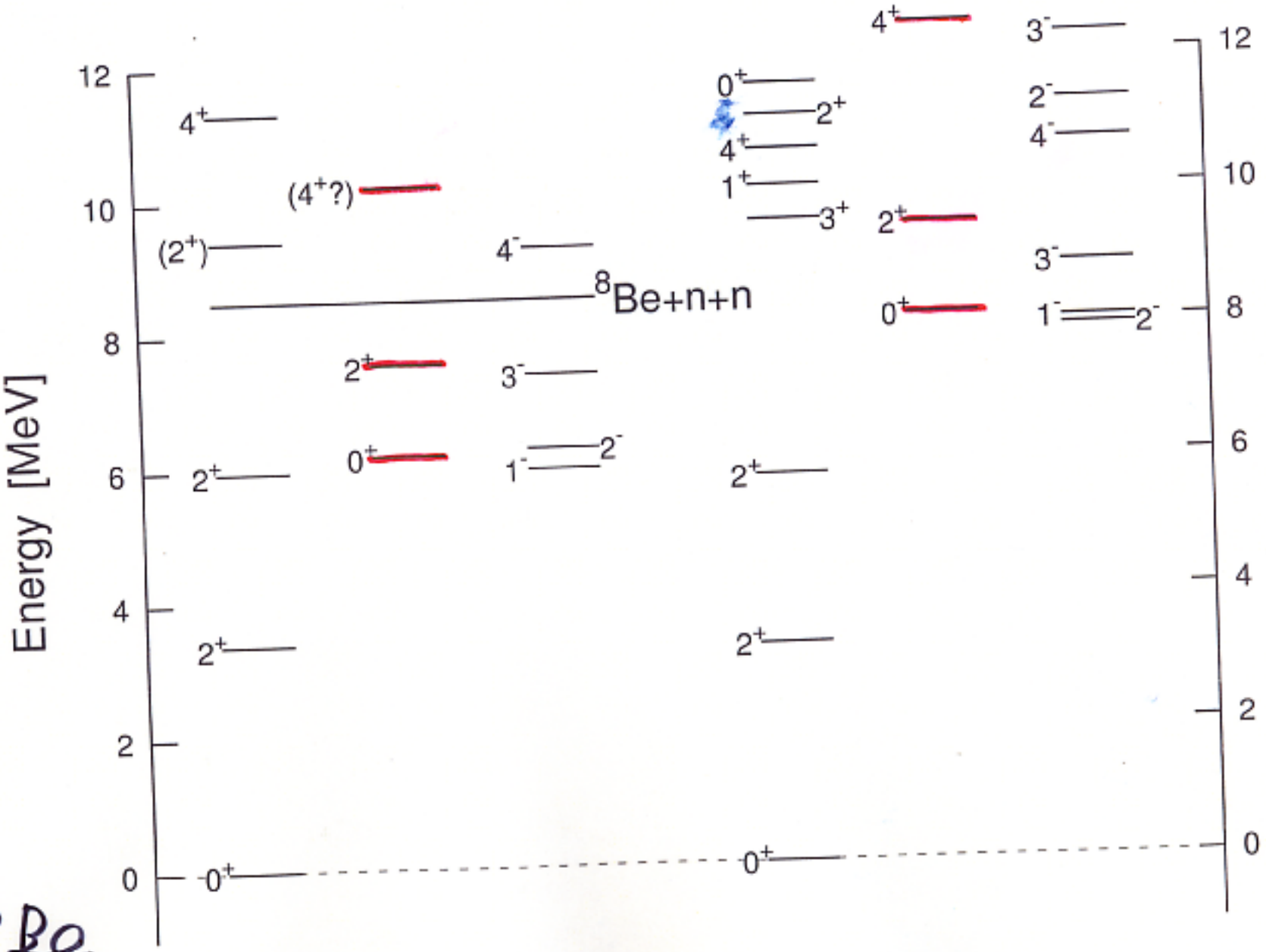

29/Jun/99

^{10}Be

α+α+n+n

N. Itagaki and S. Okabe, PRC61(2000) 044306

Freer et al.
Phys. Rev. Lett. 82 (1999)
Phys. Rev C63 (2001)

Cluster structure
around 15 MeV region

Theoretical analysis:
Ito, Phy. Rev. C62 (2000)

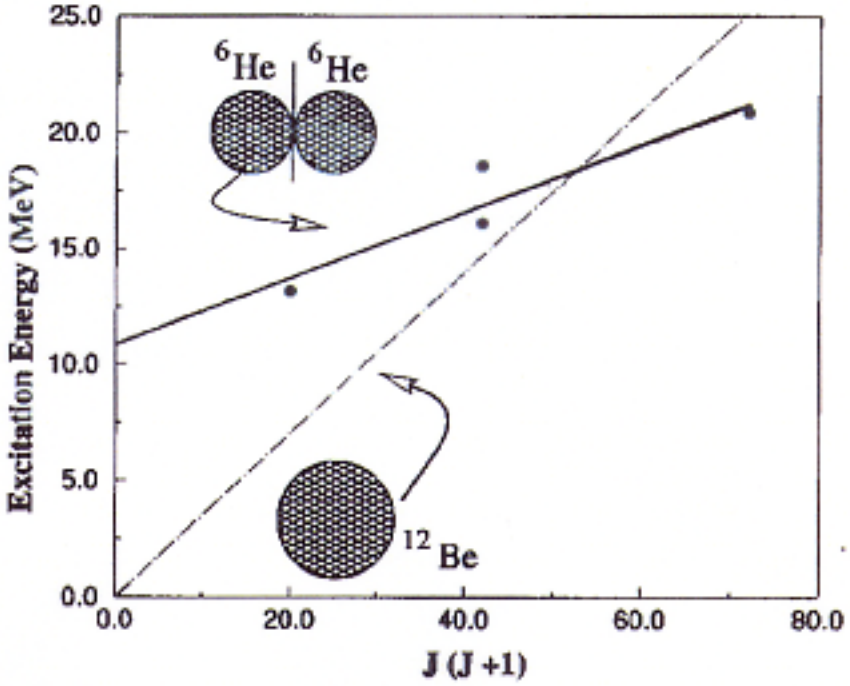

FIG. 4. The energy-spin systematics of the ^{6}He + ^{6}He breakup states (black dots). The solid line is a linear fit to the four points, and the dot-dashed line shows the extrapolated trajectory of a ground state band with a rotational energy of 350 keV.

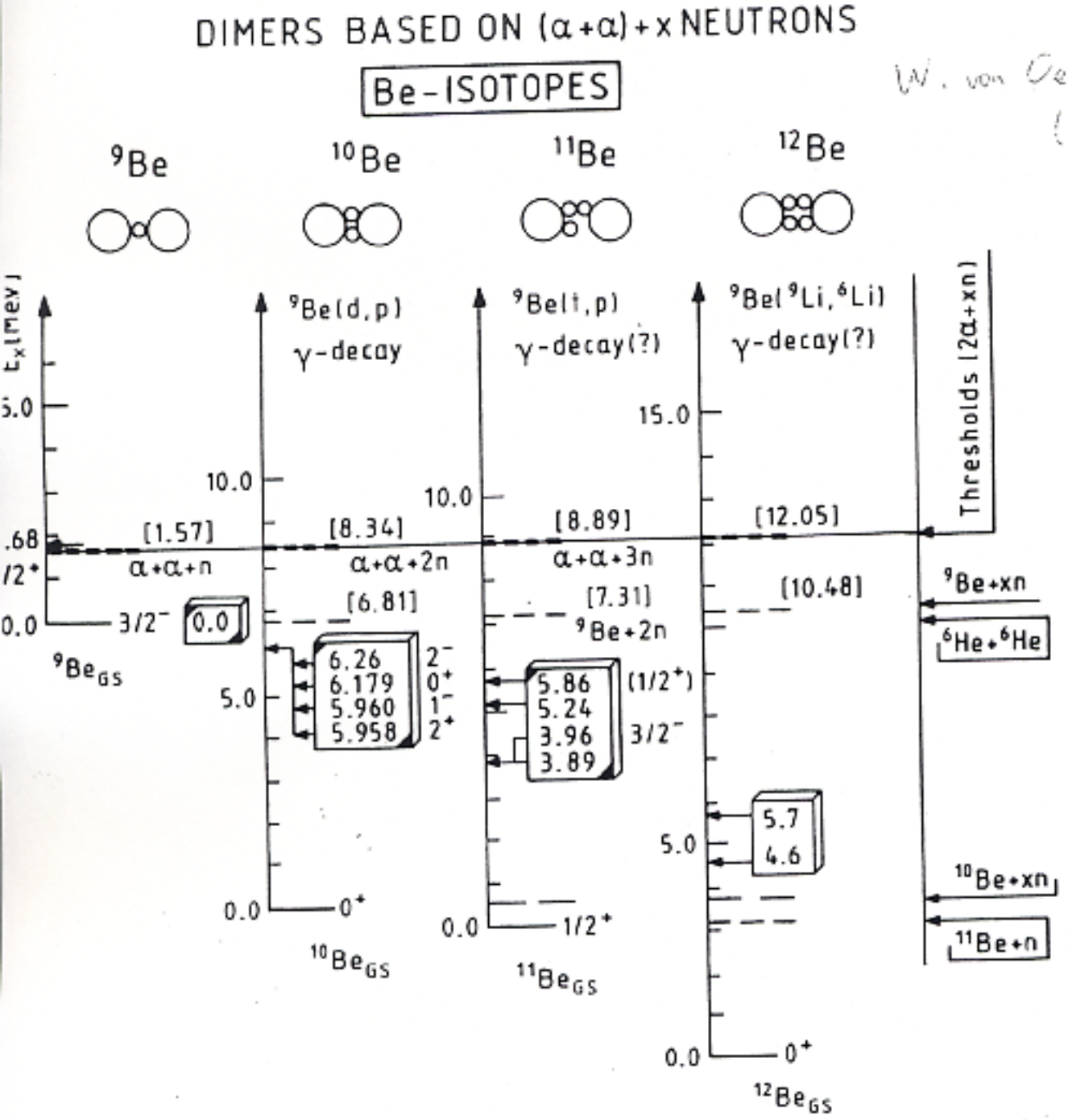

2. – Energy diagrams for dimers of the beryllium isotopes. The excitation energies (and sholds) are shown relative to the energy of the $(\alpha + \alpha + xn)$ threshold. Only the first possible eric two-center states are indicated (without rotational excitations) in boxes.

W. von Oertzen (1997)

The puzzle of ^{12}Be

Two Intrinsic Configurations

1. spherical configuration

N=8 magic number

2. deformed (clusterized) configuration

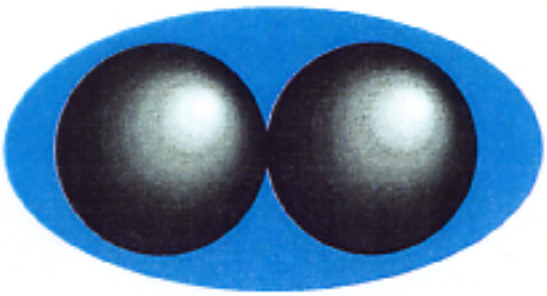

Small 0^+- 2^+ level spacing

slow β decay to ^{12}B

F.C. Barker. J. Phys G 2 L45 (1976)

T.Suzuki and T.Otsuka Phys. Rev. C56 (1997)

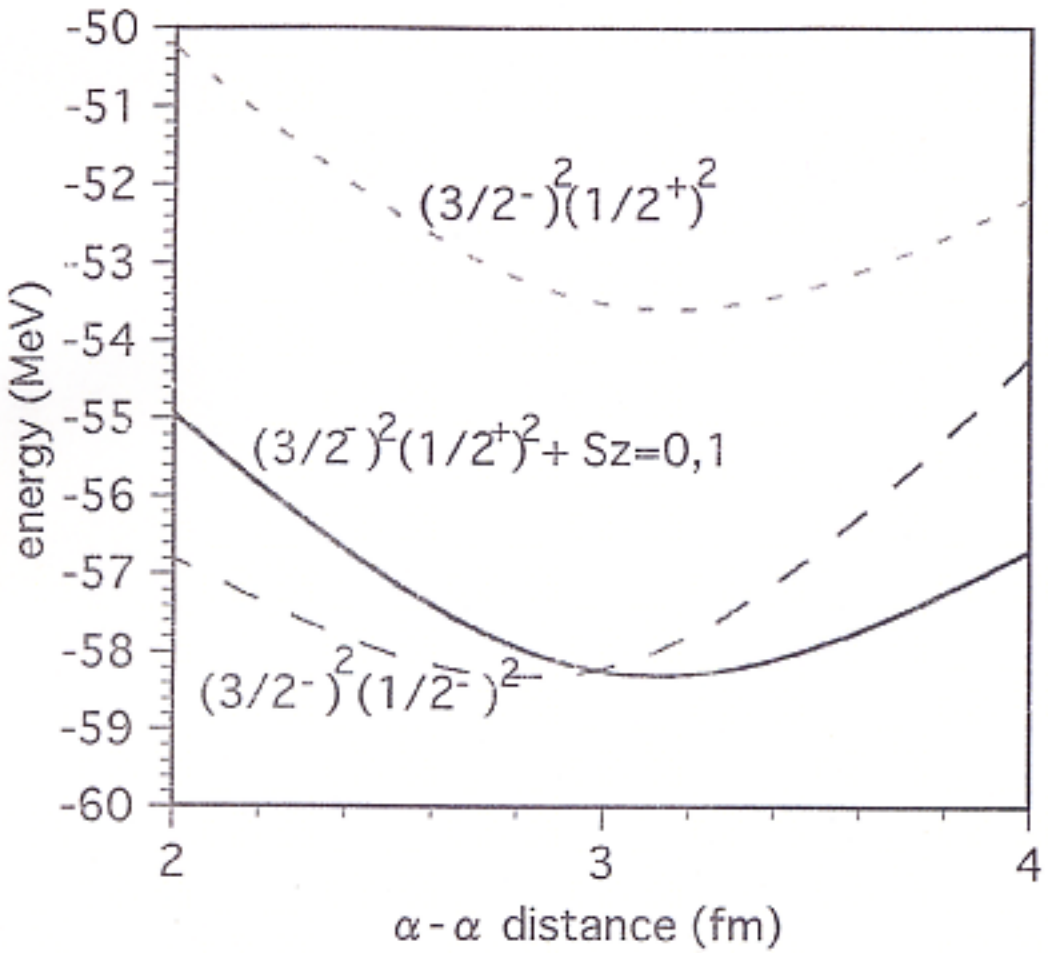

N. Itagaki. S. Okabe, and K. Ikeda
PRC62 (2000), 034301

Fig. 3

$^{12}Be = \alpha + \alpha + 4n$

Iwasaki et al.
Phys. Lett. B 481 (2000),
Phys. Lett. B 491 (2000)

β_2 was deduced

1^- state has been observed

$B(E1)=0.051\ e^2fm^2$

Theoretical analysis:
Sagawa et al.
Phys. Rev C63 (2001)

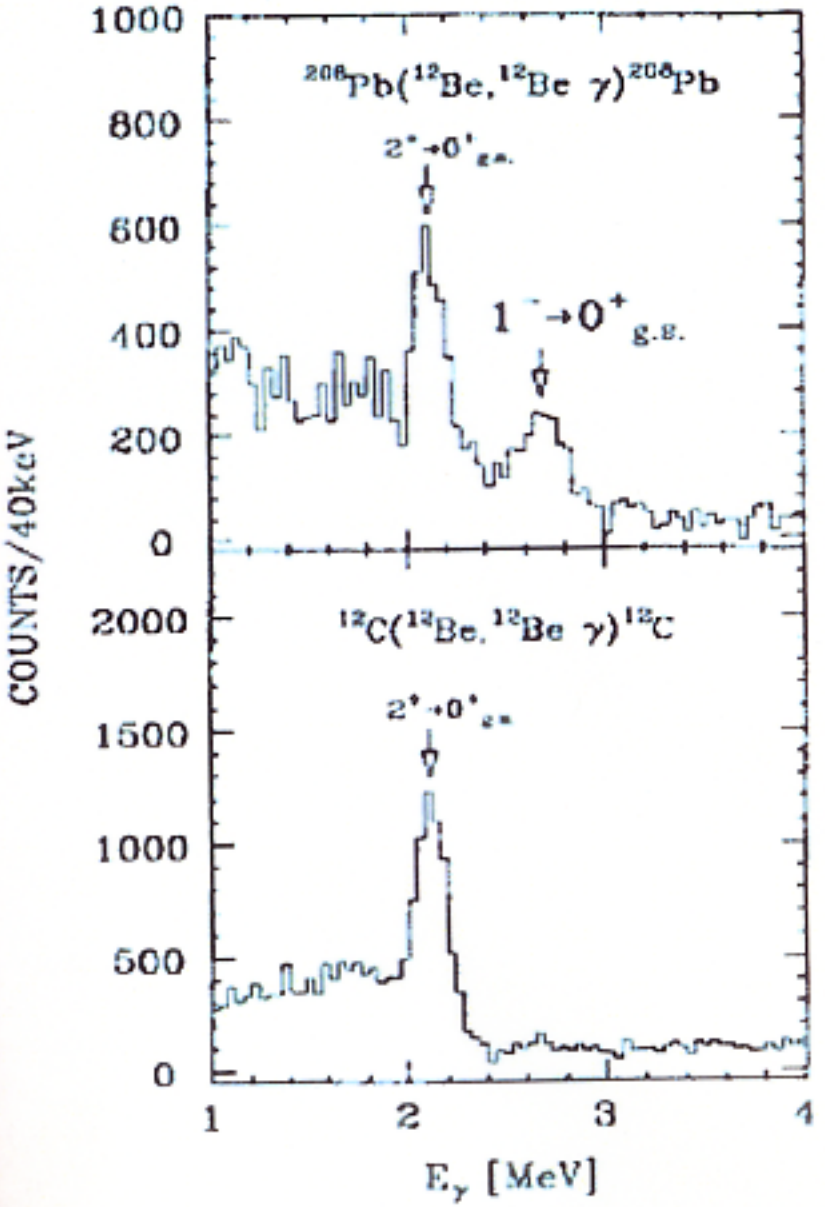

Fig. 1. Doppler-corrected γ-ray energy spectra measured in the inelastic scattering of ^{12}Be on the lead (top) and carbon (bottom) targets.

He halo

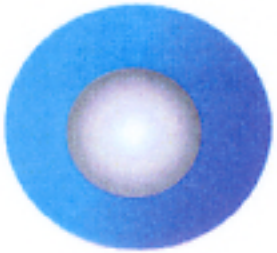

Be cluster

C polymer

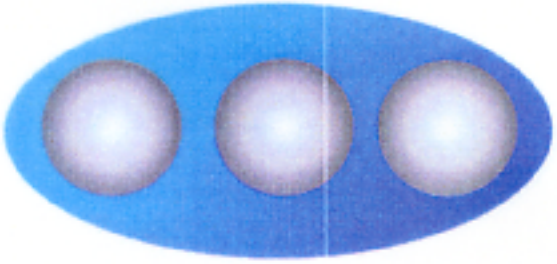

W. von Oertzen (1997)

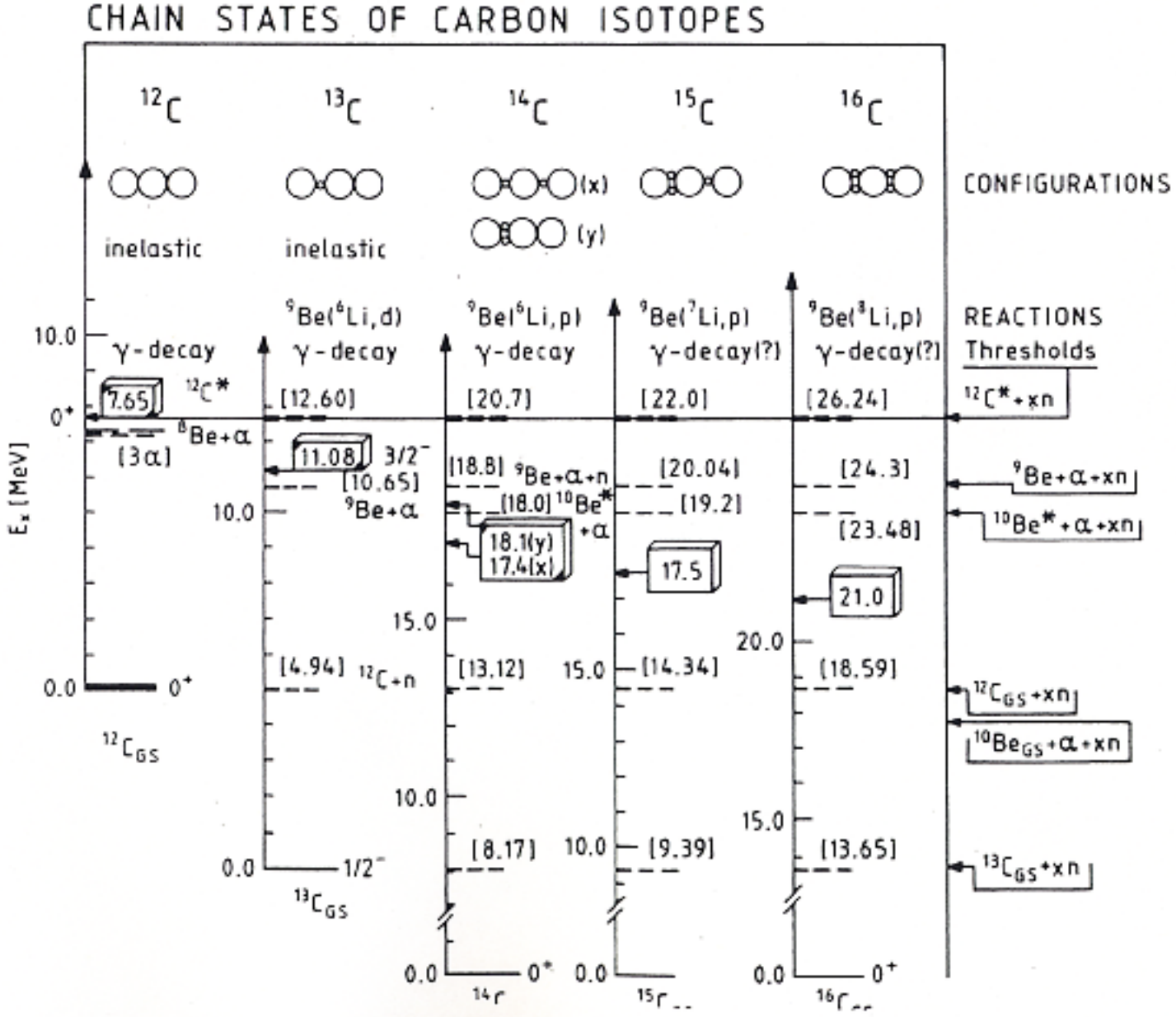

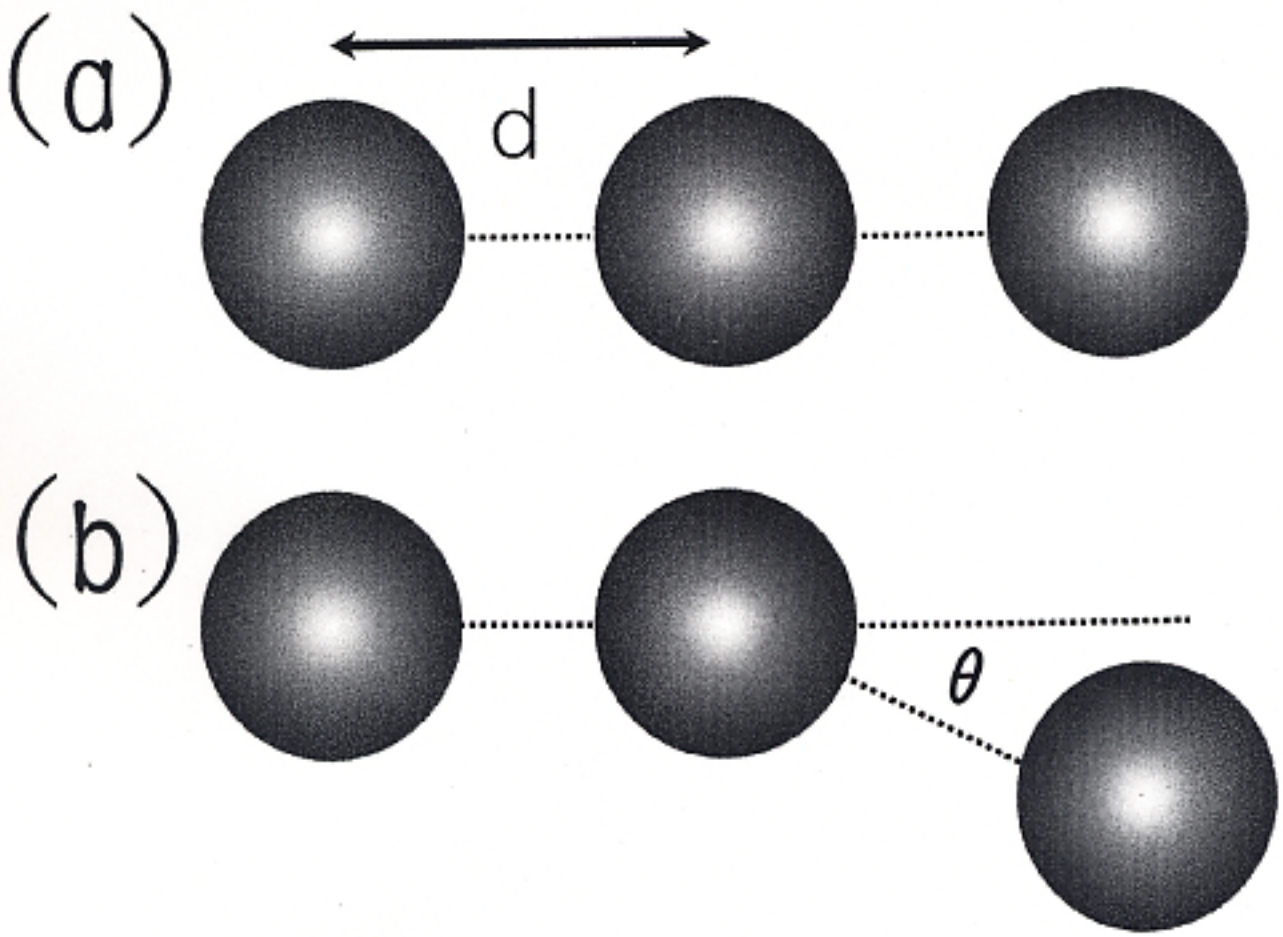
(a)
d
(b)
θ

Fig. 3

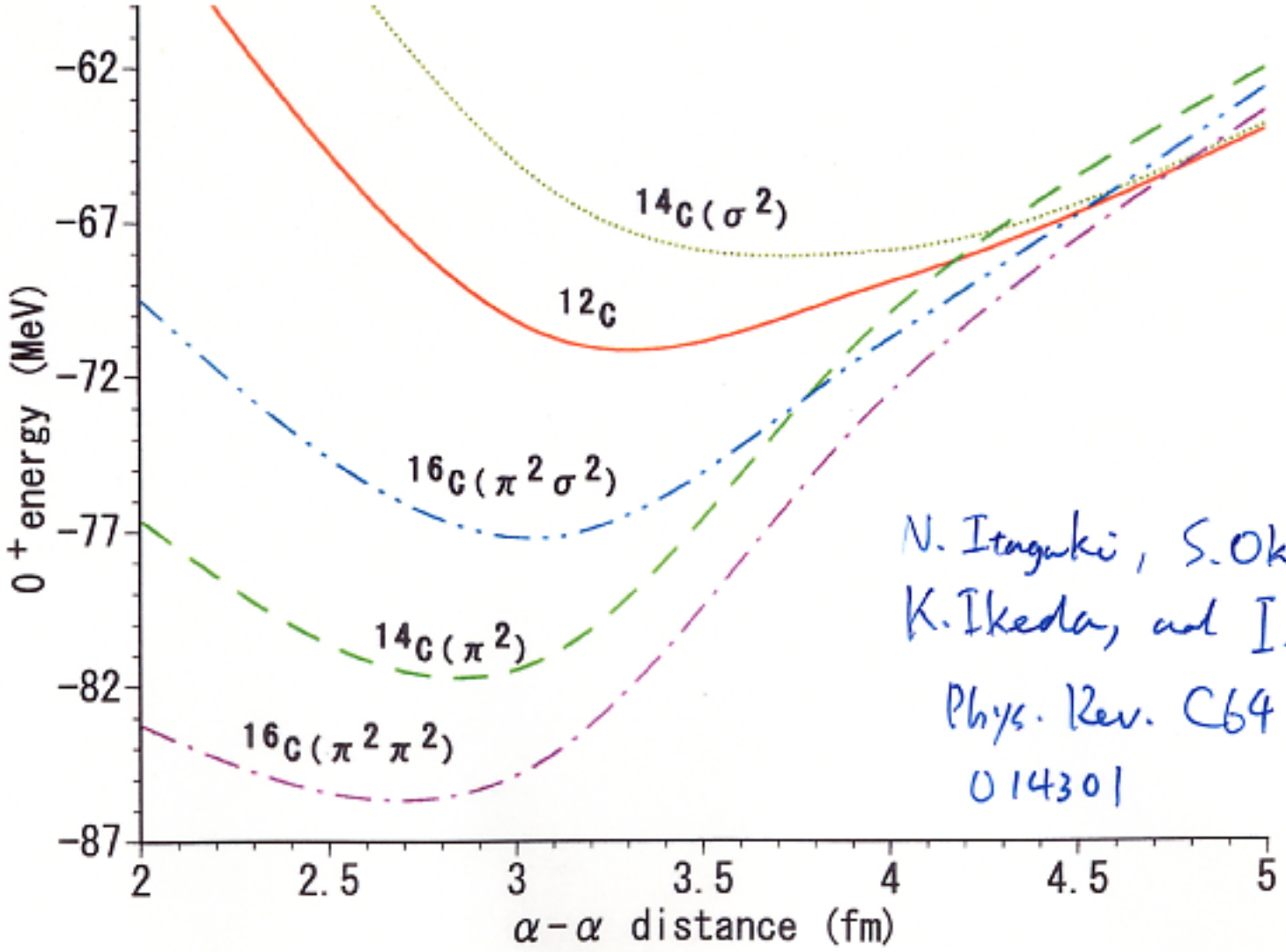

N. Itagaki, S. Okabe,
K. Ikeda, and I. Tanihata
Phys. Rev. C64 (2001),
014301

Fig. 4

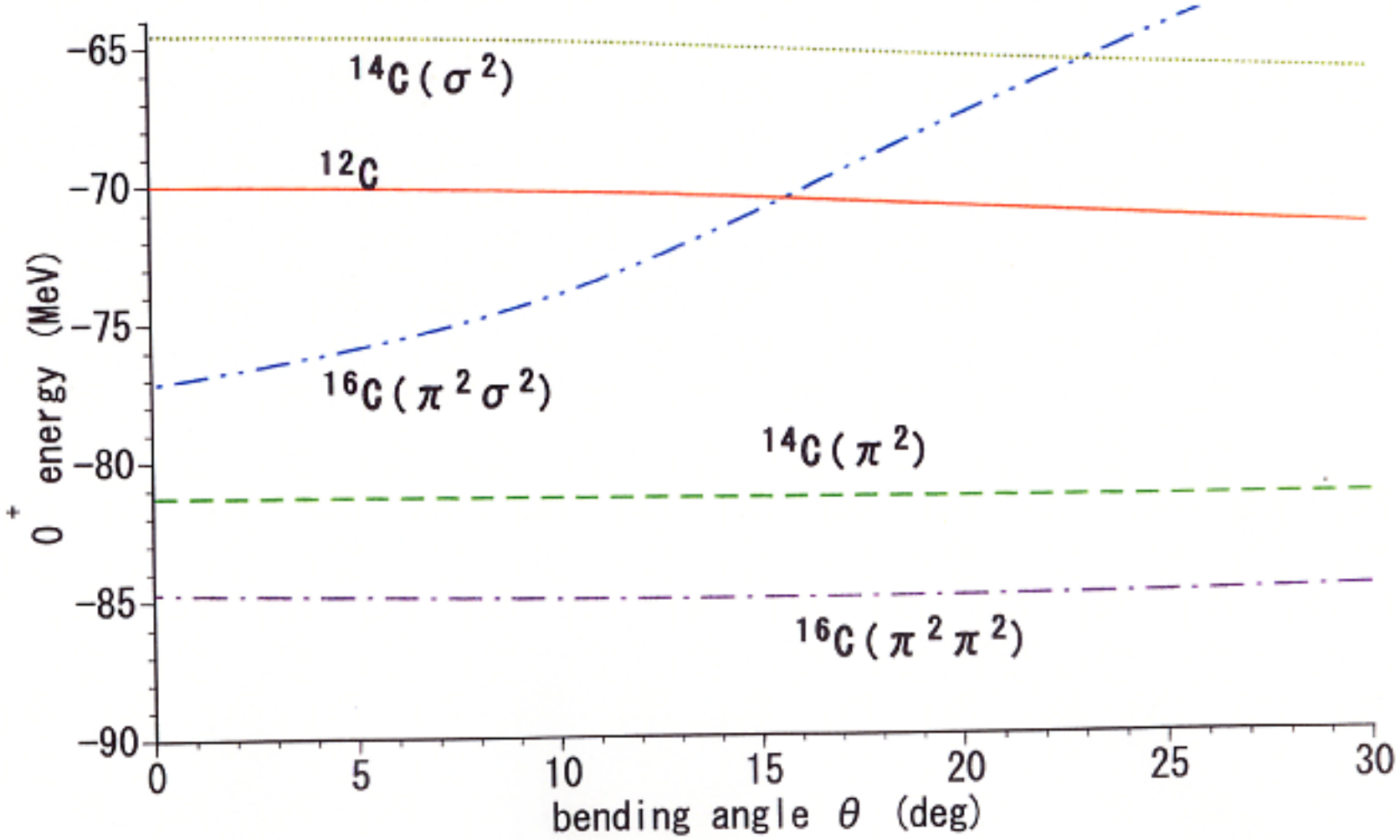

N. Itagaki, S. Okabe, K. Ikeda, and I. Tanihata
Phys. Rev. C64 (2001), 014301

Superdeformation in the $N = Z$ Nucleus ^{36}Ar: Experimental, Deformed Mean Field, and Spherical Shell Model Descriptions

C. E. Svensson,[1] A. O. Macchiavelli,[1] A. Juodagalvis,[2] A. Poves,[3] I. Ragnarsson,[2] S. Åberg,[2] D. E. Appelbe,[4] R. A. E. Austin,[4] C. Baktash,[5] G. C. Ball,[6] M. P. Carpenter,[7] E. Caurier,[8] R. M. Clark,[1] M. Cromaz,[1] M. A. Deleplanque,[1] R. M. Diamond,[1] P. Fallon,[1] M. Furlotti,[9] A. Galindo-Uribarri,[5] R. V. F. Janssens,[7] G. J. Lane,[1] I. Y. Lee,[1] M. Lipoglavsek,[5] F. Nowacki,[10] S. D. Paul,[5] D. C. Radford,[5] D. G. Sarantites,[9] D. Seweryniak,[7] F. S. Stephens,[1] V. Tomov,[9] K. Vetter,[1] D. Ward,[1] and C. H. Yu[5]

[1]*Nuclear Science Division, Lawrence Berkeley National Laboratory, Berkeley, California 94720*
[2]*Department of Mathematical Physics, Lund Institute of Technology, S-22100 Lund, Sweden*
[3]*Departamento de Física Teórica, Universidad Autónoma de Madrid, E-28049 Madrid, Spain*
[4]*Department of Physics and Astronomy, McMaster University, Hamilton, Canada L8S 4M1*
[5]*Physics Division, Oak Ridge National Laboratory, Oak Ridge, Tennessee 37831-6371*
[6]*TRIUMF, 4004 Wesbrook Mall, Vancouver, British Columbia, Canada V6T 2A3*
[7]*Argonne National Laboratory, Argonne, Illinois 60439*
[8]*Institut de Recherches Subatomiques, IN2P3-CNRS-Université Louis Pasteur, F-67037 Strasbourg Cedex 2, France*
[9]*Chemistry Department, Washington University, St. Louis, Missouri 63130*
[10]*Laboratoire de Physique Theorique, Université Louis Pasteur, F-67084 Strasbourg Cedex, France*

(Received 8 May 2000)

A superdeformed rotational band has been identified in ^{36}Ar, linked to known low-spin states, and observed to its high-spin termination at $I^{\pi} = 16^{+}$. Cranked Nilsson-Strutinsky and spherical shell model calculations assign the band to a configuration in which four pf-shell orbitals are occupied, leading to a low-spin deformation $\beta_2 \approx 0.45$. Two major shells are active for both protons and neutrons, yet the valence space remains small enough to be confronted with the shell model. This band thus provides an ideal case to study the microscopic structure of collective rotational motion.

PACS numbers: 21.10.Re, 21.60.Cs, 23.20.Lv, 27.30.+t

shown in Fig. 1(a), and a partial decay scheme for ^{36}Ar is presented in Fig. 2. Transitions denoted by diamonds in Fig. 1(a) firmly link the band to known low-spin states. For example, Fig. 1(b) shows a spectrum of the band obtained with a single gate set on the 4950-keV linking transition. The spin and parity assignments in Fig. 2 are based on angular distribution measurements which establish stretched-$E2$ character for all of the in-band and high-energy linking transitions. Two examples are shown in Figs. 1(c) and 1(d). Legendre polynomial fits to these data (solid curves) yield (a_2, a_4) coefficients of $(0.31 \pm 0.02, -0.09 \pm 0.03)$ and $(0.31 \pm 0.02, -0.08 \pm 0.02)$ for the 3352 and 4166-keV γ rays and establish the 6^+ and 4^+ states of the band. The 4951 keV 2^+ state was known from earlier ^{35}Cl$(p, \gamma)^{36}$Ar studies [16]. These studies also identified a (0^+) state at 4329 keV which, based on the regular rotational spacing, is presumed to be the SD bandhead. The γ-ray branchings from the 4^+ and 6^+ states of the band yield in-band to decay-out $B(E2)$ ratios of 148 ± 6 and 86 ± 4, consistent with strongly enhanced in-band transitions. Assuming a similar ratio of $B(E2)$'s for the 2^+ state, a 622-keV $2^+ \rightarrow 0^+$ in-band transition would be expected to carry ~0.3% of the decay intensity. The present experiment yields an upper limit of 1.0% for this unobserved branch.

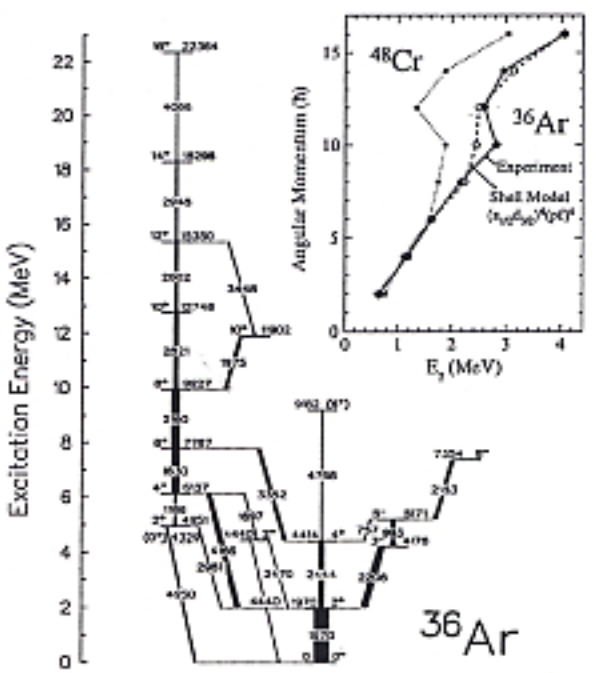

FIG. 2. Partial decay scheme for ^{36}Ar showing the superdeformed band (left). Transition and level energies are given to the nearest keV and arrow widths are proportional to transition intensities. The inset compares the experimental and shell model "backbending" plots for the SD band in ^{36}Ar, as well as experimental values for the ground band of ^{48}Cr [2–4].

P. T. P. (2001)

The single particle wave packet ψ_i consists of a spatial part, ϕ_i, spin part, χ_{si} and isospin part, $\chi_{\tau i}$. In the old version of the AMD,[7] the spatial part $\phi_i(\boldsymbol{r}_j)$ is represented in the spherical Gaussian form

$$\phi_i(\boldsymbol{r}_j) = (2\nu/\pi)^{3/4} \exp\Big\{-\nu(\boldsymbol{r}_j - \boldsymbol{Z}_i)^2\Big\}. \tag{2}$$

In the new version of AMD developed in this study, we employ the deformed Gaussian instead of the spherical one as the spatial part. This is given in Eq. (3). In the following, for simplicity, we call the old version of AMD "spherical AMD" and the new version of AMD "deformed AMD". The deformed Gaussian has an independent width parameter for each direction, x, y and z;

$$\phi_i(\boldsymbol{r}_j) = (8\nu_x\nu_y\nu_z/\pi^3)^{1/4} \exp\left\{-\sum_{\sigma=x,y,z} \nu_\sigma (r_j - Z_i)_\sigma^2\right\}. \tag{3}$$

Here, in Eqs. (2) and (3), complex variables $\boldsymbol{Z}_i$, which represent the positions of the wave packets in the phase space, are the variational parameters and depend on the individual nucleons. The width parameters ν [Eq. (2)] and ν_x, ν_y and ν_z [Eq. (3)] are also variational parameters, but are common to all nucleons. Using the deformed spatial part of the single particle wave packet, we expect the following effects. 1) When the mean field is deformed, AMD single particle wave packets will also be deformed. Therefore, with deformed AMD single particle wave packets, we

P.T.P. (2001)

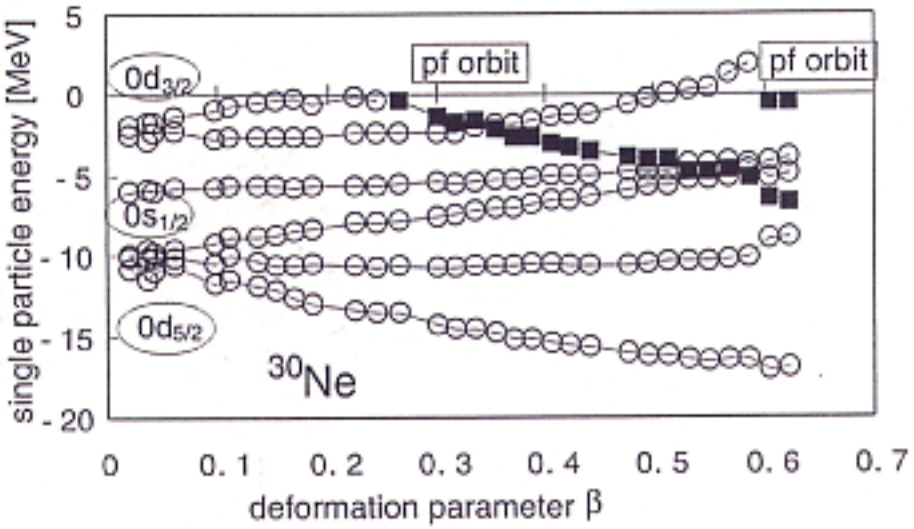

Fig. 5. Hartree-Fock single particle energies of neutrons in ^{30}Ne as functions of the deformation parameter β. Open circles (filled boxes) correspond to the plus (minus) parity orbits.

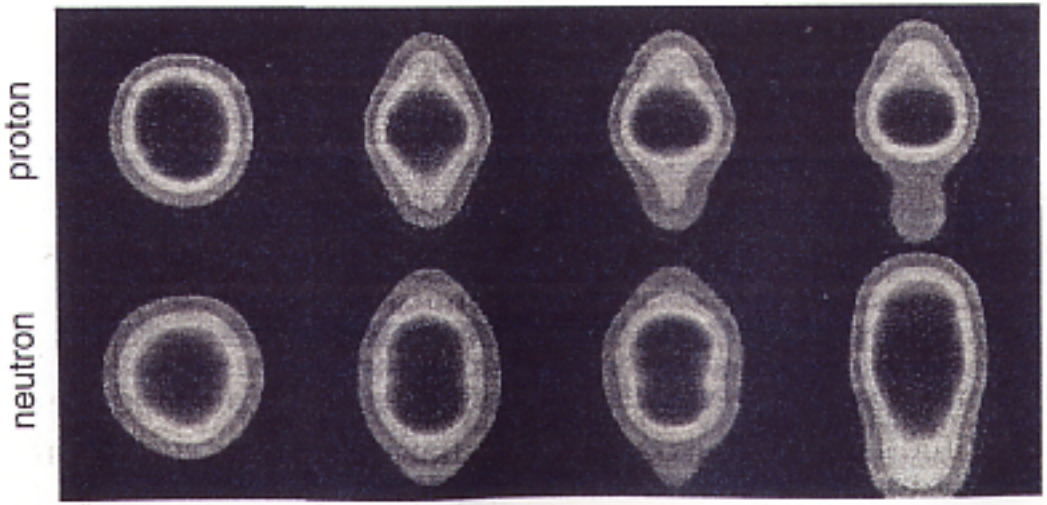

PHYSICAL REVIEW C, VOLUME 62, 014001

Quantum Monte Carlo calculations of $A=8$ nuclei

R. B. Wiringa* and Steven C. Pieper†
Physics Division, Argonne National Laboratory, Argonne, Illinois 60439

J. Carlson‡
Theoretical Division, Los Alamos National Laboratory, Los Alamos, New Mexico 87545

V. R. Pandharipande§
Physics Department, University of Illinois at Urbana-Champaign, 1110 West Green St., Urbana, Illinois 61801
(Received 7 February 2000; published 1 June 2000)

We report quantum Monte Carlo calculations of ground and low-lying excited states for $A=8$ nuclei using a realistic Hamiltonian containing the Argonne v_{18} two-nucleon and Urbana IX three-nucleon potentials. The calculations begin with correlated eight-body wave functions that have a filled α-like core and four p-shell nucleons LS coupled to the appropriate $(J^\pi;T)$ quantum numbers for the state of interest. After optimization, these variational wave functions are used as input to a Green's function Monte Carlo calculation made with a new constrained path algorithm. We find that the Hamiltonian produces a ^{8}Be ground state that is within 2 MeV of the experimental resonance, but the other eight-body energies are progressively worse as the neutron-proton asymmetry increases. The ^{8}Li ground state is stable against breakup into subclusters, but the ^{8}He ground state is not. The excited state spectra are in fair agreement with experiment, with both the single-particle behavior of ^{8}He and ^{8}Li and the collective rotational behavior of ^{8}Be being reproduced. We also examine energy differences in the $T=1,2$ isomultiplets and isospin-mixing matrix elements in the excited states of ^{8}Be. Finally, we present densities, momentum distributions, and studies of the intrinsic shapes of these nuclei, with ^{8}Be exhibiting a definite 2α cluster structure.

PACS number(s): 21.10.−k, 21.45.+v, 21.60.Ka, 27.20.+n

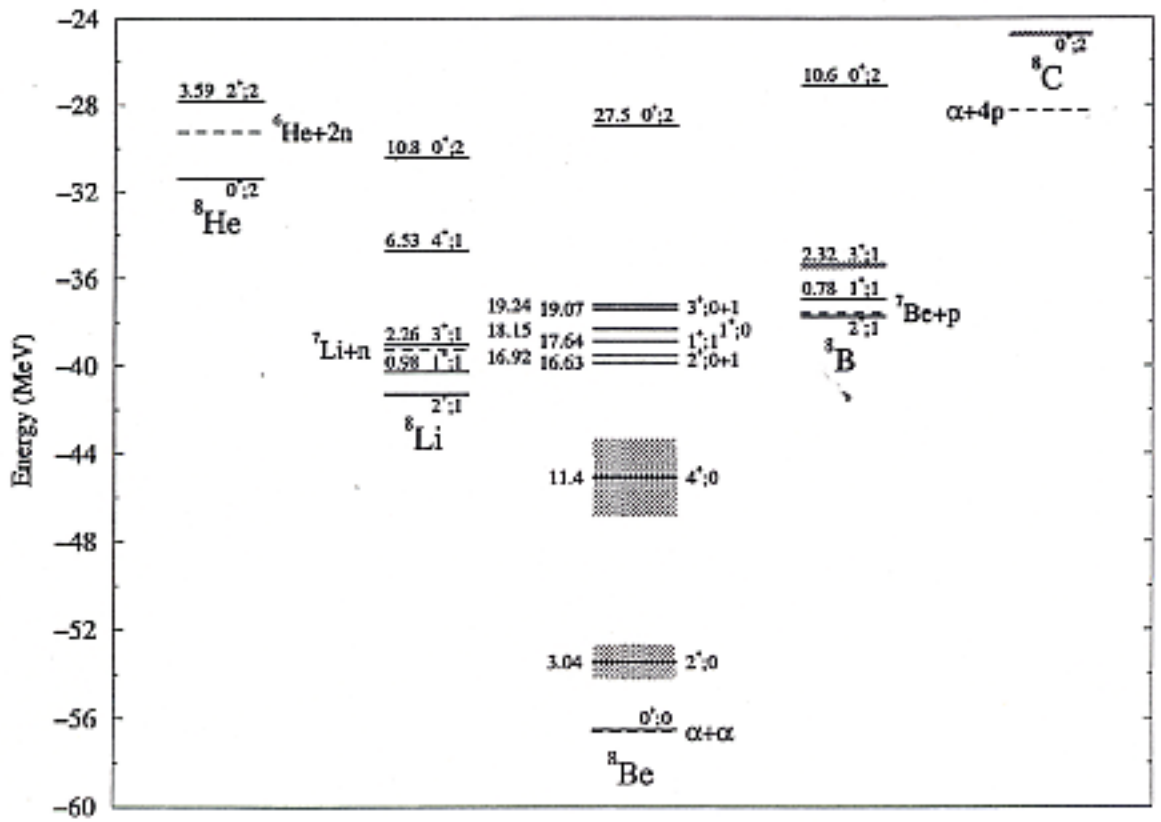

FIG. 1. The experimental spectrum for $A=8$ nuclei. All narrow low-lying states are shown, as well as the wide rotational states in ^{8}Be. Higher-lying and negative-parity states in ^{8}Be and some wider states in ^{8}Li are not shown.

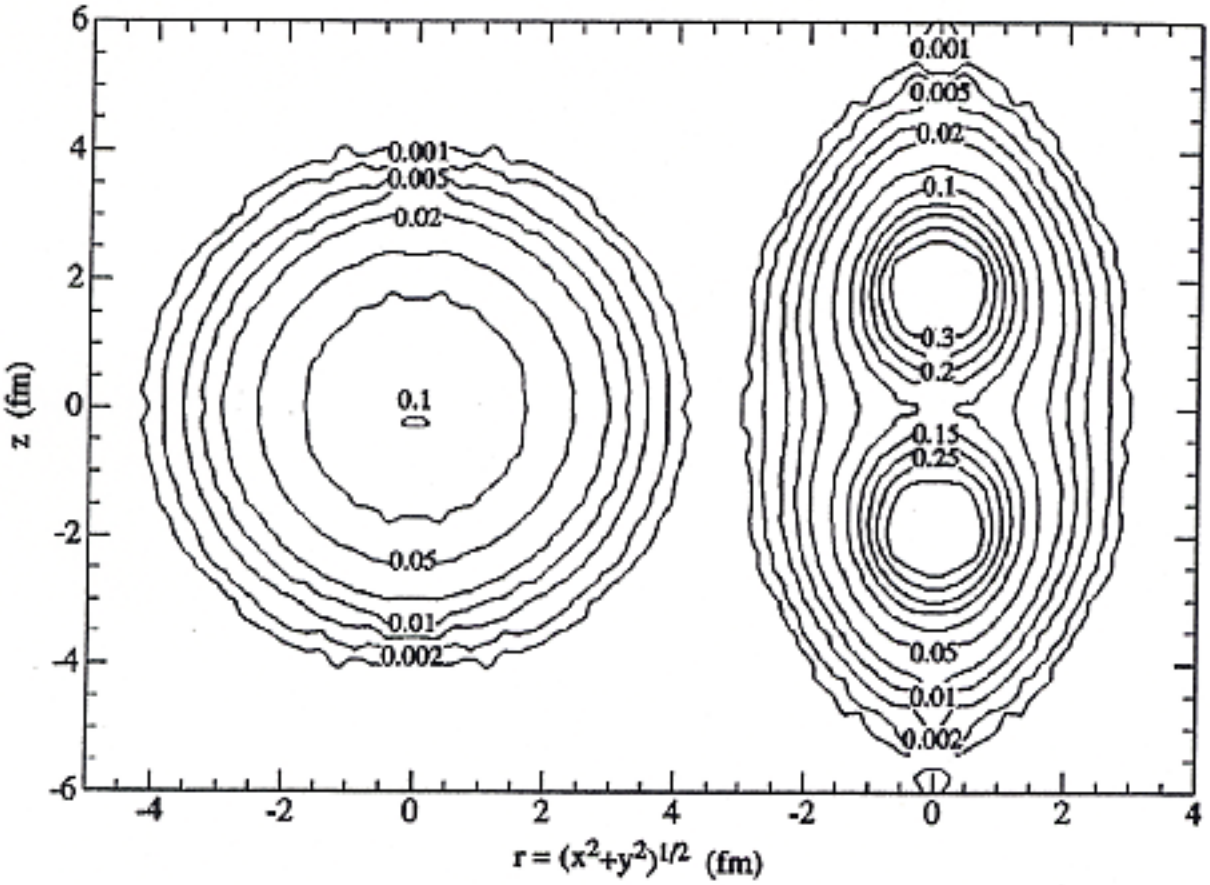

FIG. 15. Contours of constant density, plotted in cylindrical coordinates, for ^{8}Be(0^{+}). The left side is in the "laboratory" frame while the right side is in the intrinsic frame.

in Tables III and IV, for the (2^{+};0,1) and (3^{+};0,1) pairs are indeed fairly close to each other, since they have similar sizes and signs for the largest components. However, the (1^{+};0,1) states are not so similar, particularly due to the large $T=1$ ^{1}P[31] component that is not available to the $T=0$ state. This may be why the $E_{01}(1)$ is noticeably smaller, which shows up through the change in sign of the magnetic moment contribution.

Recent development and future perspctive

Cluster study has long history ～40 years

It does not mean that everything is solved

Now is the time to utilize knowlage and technic developed until now

We can discuss new phenomena related to the physics of RIB, Gamma sphere, Euro ball . . .

Theoretical iterest:

Is cluster deformation really defferent from mean-field deformation?

unified model is necessary